Title

Nongenomic Thyroid Hormone Signaling Occurs Through a Plasma Membrane–Localized Receptor

Journal

Science Signaling, 7(326)

ISSN

1945-0877

Authors

Kalyanaraman, Hema
Schwappacher, Raphaela
Joshua, Jisha
et al.

Publication Date

2014-05-20

DOI

10.1126/scisignal.2004911

Peer reviewed

HHS Public Access

Author manuscript

Sci Signal. Author manuscript; available in PMC 2019 May 07.

Published in final edited form as:

Sci Signal. ; 7(326): ra48. doi:10.1126/scisignal.2004911.

Nongenomic Thyroid Hormone Signaling Occurs Through a Plasma Membrane Receptor

Hema Kalyanaraman[1,*], **Raphaela Schwappacher**[1,*], **Jisha Joshua**[1], **Shunhui Zhuang**[1], **Brian T. Scott**[1], **Matthew Klos**[2], **Darren E. Casteel**[1], **John A. Frangos**[3], **Wolfgang Dillmann**[1], **Gerry R. Boss**[1], and **Renate B. Pilz**[1,†]

[1]Department of Medicine, University of California, San Diego, CA 92093, USA.

[2]Department of Surgery, University of California, San Diego, CA 92093, USA.

[3]La Jolla Bioengineering Institute, La Jolla, CA 92121, USA.

Abstract

Thyroid hormone (TH) is essential for vertebrate development and the homeostasis of most adult tissues, including bone. TH stimulates target gene expression through the nuclear thyroid receptors TRα and TRβ; however, TH also has rapid, transcription-independent (nongenomic) effects. We found a previously uncharacterized plasma membrane–bound receptor that was necessary and sufficient for nongenomic TH signaling in several cell types. This receptor is generated by translation initiation from an internal methionine of TRα, which produces a transcriptionally incompetent protein that is palmitoylated and associates with caveolin-containing plasma membrane domains. TH signaling through this receptor stimulated a pro-proliferative, anti-apoptotic program by increasing the intracellular concentrations of calcium, nitric oxide (NO), and cyclic guanosine monophosphate (cGMP), which led to the sequential activation of protein kinase G II(PKG II), the tyrosine kinase Src, and extracellular signal-regulated kinase (ERK)-Akt signaling. Hypothyroid mice exhibited a cGMP-deficient state with impaired bone formation and increased apoptosis of osteocytes, which was rescued by a direct stimulator of guanylate cyclase (GC). Our results link nongenomic TH signaling to a previously uncharacterized membrane-bound receptor, and identify NO synthase, GC, and PKGII as TH effectors that activate kinase cascades that regulate vital cellular processes.

INTRODUCTION

Thyroid hormones (THs), including thyroxine (T4) and its more active derivative triiodothyronine (T3), regulate gene expression by binding to nuclear thyroid receptors (TRs). The latter bind to TH-responsive elements (TREs) in target gene promoters as homodimers or as heterodimers with the retinoic acid receptor RXR (1,2). Free TRs repress

†Corresponding author. rpilz@ucsd.edu.

Author contributions: H.K. and R.S. performed most of the experimental work; J.J. and S.Z. contributed to Figs. 2 and 3, M.K. to calcium measurements, D.E.C. to vector construction, and B.T.S. to animal experiments; J.A.F. provided $NOS3^{f/f}$ mice; W.D. provided $TRA^{f/f}$ and $THRB^{f/f}$ mice; and R.B.P. and G.R.B. designed experiments, analyzed data, and wrote the manuscript.

*These authors contributed equally to the work.

Competing interests: The authors declare that they have no competing interests.

basal transcription, but the binding of TH to TRs induces a conformational change, releasing co-repressors, recruiting co-activators, and activating transcription of target genes within hours to days (1). Two TR genes (*THRA* and *THRB)* generate multiple TRα- and TRβ-encoding mRNAs; some encode proteins that do not bind to TH, but are transcriptional antagonists (1,3).

TH has transcription-independent, nongenomic effects that occur within seconds to minutes through poorly defined mechanisms (1). In myocytes and neurons, TH increases the concentration of free intracellular calcium (Ca^{2+}), which contributes to positive cardiac inotropy and chronotropy, whereas in vascular cells, TH activates endothelial nitric oxide synthase 3 (NOS3), which leads to vasodilation (4–6). In many cell types, TH activates extracellular signal– regulated kinases 1 and 2 (ERK½), thereby increasing cell proliferation (1,7–9). ERK activation is thought to occur through the low-affinity binding of T3 or T4 to the integrin $\alpha_v\beta_3$ (1,7,10); however, TH binds to cell membranes with high-affinity, and sub-nanomolar concentrations of T3 stimulate ion channels in the plasma membrane (1,2,4,11). These data suggest that a high-affinity TH receptor exists in the plasma membrane; however, it has not yet been identified.

Among its many physiological functions, TH regulates bone growth and remodeling, stimulating osteoclasts to resorb bone and osteoblasts to produce new bone. Osteoclast stimulation occurs largely through the production of the osteoclast-stimulating cytokine RANKL (receptor activator of nuclear factor-κB ligand) by osteoblasts (12). Excess TH leads to high bone turnover osteoporosis because osteoclasts outpace osteoblasts, whereas a decreased TH concentration leads to brittle bones from decreased bone turnover because of reduced osteoblast and osteoclast activities (12). Both states lead to increased bone fractures, and even subclinical changes in thyroid status affect bone metabolism and may increase fracture risk in older people (12). We previously showed that NO stimulates ERK and Akt in osteoblasts and osteocytes (13–15). Here, we used osteoblasts as a model system to study nongenomic TH signaling. We found that TH activated the NO-cyclic guanosine monophosphate (cGMP)-protein kinase G (PKG) signaling cascade through a previously uncharacterized, plasma membrane–associated TRα isoform, thereby stimulating Src, ERK, and Akt. This signaling mechanism occurs in multiple cell types, and is physiologically relevant, enhancing osteoblast proliferation and survival in vitro and bone formation in vivo.

RESULTS

Nongenomic TH signaling requires a TRα isoform

In human primary osteoblasts (hPOBs) and mouse osteoblast-like MC3T3 cells, 1 nM T3 stimulated the phosphorylation (and activation) of Src, ERK½, and Akt within 2 to 5 min, with the extent of phosphorylation returning to basal amounts at 20 to 30 min after treatment (Fig. 1A and fig. S1, A and B). Concentrations of T3 as low as 10^{-11}M were effective, whereas 10^{-8} to 10^{-7} M T4 was required for kinase activation; the inactive T3 isomer reverse T3 (rT3) was without effect at 10^{-7} M (Fig. 1B and fig. S1C). These results suggest the involvement of a classic TR, because T3 and T4 bind to TRs at sub-nanomolar (KD < 10^{-9}M) and high-nanomolar (~10^{-7} M) concentrations, respectively (16). To assess whether TRα or TRβ mediated the effects of TH, we isolated POBs from mice with floxed *THRA* or

THRB alleles. That the *THRA*$^{f/f}$ and *THRB*$^{f/f}$ cells were osteoblasts was demonstrated by their differentiation potential (fig. S1A), and CRE-mediated recombination reduced the abundances of TRα and TRβ mRNAs by ~70% (fig. S1D). Depletion of TRα, but not TRβ, prevented the T3-dependent phosphorylation of ERK and Akt, whereas reconstituting TRα-depleted cells with the TRα1 receptor protein restored their responsiveness to T3 (Fig. 1, C and D, and fig. S1E). We found similar results in experiments with MC3T3 cells that were treated with TRα- and TRβ-specific small interfering RNAs (siRNAs); however, TRβ1 could not substitute for TRα1 in TRα-depleted cells (Fig. 1E and fig. S1, F and G).

Identification of previously uncharacterized TRα isoforms and their functions in nongenomic TH signaling

Multiple TRα forms are expressed from the *THRA* gene through differential splicing (including TRα1 and TRα2) and transcription from an intronic promoter (TRΔα1 and TRΔα2), but only the full-length TRα1 mRNA encodes a ligand-binding receptor (Fig. 2A) (3). We found four TRα1 isoforms of ~30, 33, 43, and 48 kD in size in MC3T3 cell extracts, which were reduced markedly in abundance in cells transfected with TRα-specific siRNA, but were restored in cells infected with adenovirus encoding siRNA-resistant rat TRα1 (Fig. 2B and fig. S2A). The TRα1 antibody does not recognize TRβ (fig. S2B). These four isoforms were also observed in cells transfected with plasmid encoding FLAG-tagged TRα1 and were detectable over a 10-fold range of abundance (Fig. 2C, fig. S2C). At the lowest amount of transfected DNA, the amount of protein was similar to that of endogenous TRα1 (fig. S2C), with the epitope-tagged proteins migrating with a higher apparent molecular weight (fig. S2D). In contrast, cells transfected with plasmid encoding FLAG-tagged TRβ1 produced only a single protein (fig. S2B).

The 48-kD TRα1 isoform represents the full-length receptor, and the 43-kD isoform is likely mitochondrial TRα1, which initiates translation from Met^{39} and functions as a mitochondrial transcription factor (17). We hypothesized that the other two isoforms originated from additional internal translation initiation codons. Because translation initiation from an AUG codon depends primarily on the surrounding nucleotide sequence, and the selection of secondary sites is stronger in genes with weak primary start sites, we focused on Met^{120}, Met^{122} and Met^{150}, because their codons are in the context of perfect Kozak consensus sequences, whereas Met^{1} and Met^{39} are not (Fig. 2A) (18). Mutating Met$^{120/122}$ or Met^{150} to isoleucine eliminated the 33- and 30-kD isoforms, respectively, whereas mutating all three methionines (Mut x3) eliminated both isoforms (Fig. 2D). Deleting codons 1 to 119 (Δ119) or 1 to 149 (Δ149) produced the expected peptides initiated from Met$^{120/122}$ and/or Met^{150}, respectively, whereas deleting codons 1 to 119 from the Ile^{150} construct yielded the expected single peptide (Fig. 2D). Thus, we found that the 30- and 33-kD TRα1 isoforms were produced from internal translational start codons.

To determine whether the 30-kD, 33-kD, or both TRα1 isoforms mediated nongenomic TH signaling, we reconstituted TRα-depleted MC3T3 cells with several TRα1 constructs. The Δ119 and Δ149 TRα1 constructs restored T3-dependent ERK and Akt activation, but a Δ119^{PH} mutant construct did not (Fig. 2E). The latter mutant contains a histidine substitution for Pro^{398}, which abolishes T3 binding at physiological concentrations (19).

Full-length TRα1 constructs containing either $Ile^{120/122}$ or Ile^{150} supported T3-dependent ERK and Akt activation as efficiently as did the wild-type receptor, but the Mut x3 protein containing all three isoleucines did not (Fig. 2F). The Mut x3 protein had normal transcriptional activity, whereas the Δ119 and Δ149 mutants were not transcriptionally active and suppressed T3-induced transcription by endogenous TH receptor or by overexpressed wild-type TRα1 in transfected cells (Fig. 2G and fig. S2E). This dominant-negative effect is likely a result of hetero-dimerization between the wild-type and truncated receptors, with the latter lacking DNA-binding and transactivation domains. Nongenomic TH signaling by the TRα1-Δ149 mutant also occurred in NIH-3T3 fibroblasts and MDA-MB231 breast cancer cells. T3-dependent ERK and Akt activation was blocked by siRNA-mediated loss of TRα and was restored by reconstituting the cells with TRα1-Δ149 (fig. S2, F to I). Thus, the 30-kD, 33-kD, or both TRα1 isoforms are necessary and sufficient to mediate nongenomic TH signaling.

The 30-kD TRα isoform (p30 TRα1) is palmitoylated and co-localizes with caveolin-1 and NOS3 in plasma membranes

The 30-kD, but not the 33-kD, TRα1 isoform was present in osteoblast membrane fractions. It co-migrated with the peptide initiated from Met^{150} and was depleted in cells transfected with TRα-specific siRNA (Fig. 3A and fig. S3A). This protein, which we refer to as p30 TRα1, was retained on T3-sepharose, even in the absence of cofactors, but was not retained on control resin (Fig. 3B and fig. S3, B to D). It was also detected by a second antibody directed against a different C-terminal TRα1 epitope (fig. S3B). Similar results were obtained in experiments with NIH-3T3 fibroblasts (Fig. 3C and fig. S3E).

Through gradient centrifugation, we isolated light buoyancy membrane lipid rafts—cholesterolrich plasma membrane micro-domains that contain caveolin-1 and function as unique signal transduction platforms (20). p30 TRα1 tracked with caveolin-1 in lipid rafts from murine POBs, whereas in MC3T3 cells expressing Myc-tagged p30 TRα1, p30 TRα1 tracked with caveolin-1, NOS3, PKG II, and Src (Fig. 3, D and E). The association of proteins with plasma membranes can be mediated by posttranslational lipid modifications, and sequence analysis of p30 TRα1 predicted that Cys^{254}, Cys^{255}, or both were potential palmitoylation sites (CSS-Palm 3.0). We found that ^{14}C-palmitic acid was incorporated into p30 TRα1, and that the palmitoylation inhibitor 2-bromo-palmitate and the cholesterol-depleting agent methyl-β-cyclodextrin blocked T3-dependent ERK and Akt activation (Fig. 3F and fig. S3, F and G). A mutant p30 TRα1 in which Cys^{254} and Cys^{255} were mutated to alanines did not reconstitute TH signaling in TRα-depleted cells and was not localized to the plasma membrane, whereas a mutant p30 TRα1 in which a neighboring cysteine (Cys^{244}) was changed to an alanine was fully functional (Fig. 3, G and H). Thus, Cys^{254}, Cys^{255}, or both are required for the membrane targeting of p30 TRα1 and its signaling. In contrast, the myristoylation inhibitor 2-hydroxymyristic acid had no effect on the membrane localization of p30 TRα1, although it blocked the membrane association of PKGII (fig. S3H).

To assess whether p30 TRα1 colocalized with caveolin-1, we used two approaches in MC3T3 cells expressing epitope-tagged p30 TRα1. First, we used a proximity ligation assay, by which the juxta-position of two antibodies covalently linked to

oligodeoxynucleotides enables the formation of circular DNA strands and replication by a rolling-circle amplification reaction. With this assay, we observed punctate signals of amplified DNA (red) on the plasma membrane, indicating that p30 TRα1 and caveolin-1 were within ~40 nm of each other (Fig. 3I) (21). Second, through double immunofluorescence staining, we found that p30 TRα1 co-localized with caveolin-1 on the plasma membrane (Fig. 3, J and K). Thus, p30 TRα1 associates with caveolin-1–containing membrane microdomains, which contain NOS3, PKGII, Src, and other signaling molecules (20,22).

TH activates ERK and Akt through Ca^{2+}, NOS3, membrane-bound PKGII, Src, and the integrin β_3 subunit

TH activates NOS1 and NOS3 isoforms in several cell types (5,6), and the NO-dependent activation of soluble guanylate cyclase (sGC) and PKG leads to the activation of Src, ERK, and Akt in osteoblasts (Fig. 4A) (15). Thus, we hypothesized that TH signals to ERK and Akt through the NO-cGMP-PKG pathway. We found that T3 stimulated osteoblasts to produce NO, and that this required TRα, but not TRβ (Fig. 4B). T3 increased NO production in *THRA*$^{f/f}$ POBs exposed to control virus but not CRE virus, whereas in *THRB*$^{f/f}$ POBs, T3 increased NO production in the presence or absence of CRE (Fig. 4B and fig. S1D). In TRα-depleted osteoblasts, reconstitution of cells with p30 TRα1 restored T3-dependent NO production, whereas Mut x3 TRα had no effect (Fig. 4C and fig. S4A. The T3-dependent increase in NO was blocked by the nonselective NOS inhibitor L-NAME and by the extracellular Ca^{2+} chelator EGTA (Fig. 4D and fig. S4B). EGTA blocked the rapid T3-dependent increase in intracellular Ca^{2+} (Fig. 4E). These data suggest that T3 activates Ca^{2+}-dependent NOS1 or NOS3. We found that NOS3 was the target, because T3 failed to increase NO production in NOS3-deficient POBs, and NOS3 was required for the T3-dependent activation of PKG, ERK, and Akt (Fig. 4, F and H, and fig. S4A). NOS3 can also be activated by its phosphorylation by Akt on Ser^{1177}, and we found that the phosphatidylinositol 3-kinase (PI3K) inhibitor LY294002 blocked T3-dependent Akt activation and NOS3 phosphorylation on Ser^{1177}, as well as reduced NO production (Fig. 4, D and G and fig. S4C). We conclude that T3 activates NOS3 both directly by increasing the concentration of intracellular Ca^{2+}, and indirectly through the Akt-dependent phosphorylation of Ser^{1177} (23).

To assess whether sGC or PKG were required for nongenomic TH signaling, we used pharmacological activators or inhibitors of both enzymes (Fig. 4A), and found that activators stimulated, whereas inhibitors blocked, the T3-dependent activation of Src, ERK, and Akt (Fig. 4, I and J, and fig. S4D). To determine which PKG isoform was involved, we used an siRNA-based approach. Depleting PKGI had no effect, but depleting PKGII completely blocked the T3-dependent activation of Src, ERK, and Akt (Fig. 4, K and L). Signaling was restored in cells reconstituted with wild-type PKGII, but not with a myristoylation-deficient mutant PKGII (G2A), which does not bind to the plasma membrane (Fig. 4M) (14). Moreover, 2-hydroxymyristic acid blocked the T3-dependent activation of ERK and Akt (fig. S4E).

We previously demonstrated that PKGII activates Src bound to the cytoplasmic tail of the integrin β_3 subunit through stimulation of the Src homology domain-2-containing phosphatases SHP1 and SHP2 (14). Here, we found that the T3-induced activation of ERK and Akt required Src, SHP-2, and the integrin β_3 subunit (fig. S4, F and G). The latter finding may explain the role of the integrin β_3 subunit in T3-dependent ERK activation (7,10). Consistent with published data (10), we found that integrin $\alpha_v\beta_3$ bound to T3-sepharose, but the presence or absence of $\alpha_v\beta_3$ did not affect the binding of T3 to p30 TRα1 (fig. S4, H and I). Depletion of the β_3 integrin subunit reduced T3-stimulated NO production by ~50%, likely because the stimulation of NOS3 by T3 requires β_3-dependent Akt activation in addition to Ca^{2+} influx (fig. S4, C, F, and J). These data suggest a previously uncharacterized signaling pathway from p30 TRα1 to ERK and Akt through Ca^{2+}, NOS3, PKGII, and Src.

Nongenomic TH signaling through the p30 TRα1–NO–cGMP pathway stimulates cell proliferation and survival

Because ERK and Akt are linked to cellular proliferation and survival, we investigated whether TH regulated the proliferation and survival of osteoblasts through the p30 TRα1–NOS3 pathway. T3 increased the number of POBs and MC3T3 cells in S-phase by two-to three-fold, with TRα, but not TRβ, being required for the increased DNA synthesis (Fig. 5, A and B, and fig. S5A). In TRα-depleted osteoblasts, reconstitution with full-length, wild-type TRα1 completely restored proliferation, whereas reconstitution with p30 TRα1 or the full-length Mut x3 TRα1 only partly restored proliferation (Fig. 5B and fig. S5A). These data suggest that membrane-initiated T3 signaling through p30 TRα1 cooperates with nuclear T3 signaling to promote osteoblast growth. Because the CRE-mediated reduction of TRα abundance did not affect basal osteoblast proliferation in hormone-free medium, the amount of apo-TRα did not appear to influence osteoblast proliferation under the experimental conditions. T3-dependent proliferation required NOS3, and was blocked by inhibiting PKG (with Rp-CPT-PET-cGMPS), MEK-ERK (with the MEK inhibitor U0126), or PI3K-Akt signaling (with the PI3K inhibitor LY294002) (Fig. 5, C and D and fig. S5B).

T3 protected POBs and osteocyte-like MLO-Y4 cells from death induced by serum-starvation or treatment with the topoisomerase inhibitor etoposide, respectively; however, protection was lost by depleting TRα in $THRA^{f/f}$ POBs, but was completely restored by reconstituting the cells with p30 TRα1 (Fig. 5E and fig. S5C). T3-mediated protection from serum starvation required NOS3, because T3 had no effect in CRE-treated *NOS3*$^{f/f}$ POBs (Fig. 5, F and G). The NO-independent sGC stimulator cinaciguat bypassed the requirement for T3 and NO and protected *NOS3*$^{f/f}$ POBs in the absence and presence of CRE (Fig. 5F). PKG, MEK, and PI3K inhibitors prevented the anti-apoptotic effects of T3 in hPOBs and MLO-Y4 cells (Fig. 5H and fig. S5C). Thus, the pro-proliferative and anti-apoptotic effects of T3 in osteoblasts require signaling by p30 TRα1 through NO-cGMP, PKG, MEK-ERK, and PI3K-Akt.

In mPOBs and MC3T3 cells, T3 increased the expression of proliferation-associated *fos* family genes (*c-Fos* and *Fosl1*), but this effect was blocked by L-NAME, ODQ, Rp-CPT-PET-cGMPS, or U0126 (Fig. 5I and fig. S5D), consistent with the expression of these genes

being regulated by NO-cGMP-PKG and ERK-dependent pathways (13). L-NAME also prevented the T3-dependent increase in the abundance of osteocalcin (*Bglap2*) and osteopontin (*Ssp1*) mRNAs in differentiating mPOBs, but it did not reduce the T3-dependent increase in RANKL (*Tnfsf11*) mRNA abundance, consistent with RANKL being a direct genomic TR target (Fig. 5I) (24). Expression of the RANKL antagonist osteoprotegerin (*Tnfrsf11b*) was unaffected by T3 or L-NAME. Thus, the T3-dependent regulation of genes associated with the proliferation and differentiation of osteoblasts required NO signaling, whereas the T3-dependent production of RANKL was independent of NO.

Hypothyroid mice are cGMP-deficient, and increasing cGMP abundance improves bone formation and prevents apoptosis of osteocytes

Hypothyroidism is characterized by reduced bone turnover because of decreased osteoblast and osteoclast activities (12). To determine the physiological relevance of cGMP-dependent TH actions in vivo, we examined the skeletal effects of the NO-independent sGC stimulator cinaciguat in hypothyroid mice. Cinaciguat is a prototype of a new class of cGMP-enhancing agents that are in clinical development (25). Mice were fed an iodine-deficient diet containing the deiodinase inhibitor propylthiouracil (PTU) for four weeks, and they received daily injections of vehicle or cinaciguat, the latter at a dose that transiently reduces systolic blood pressure (25). The iodine-deficient, PTU-containing diet induced severe hypothyroidism as evidenced by the reduced serum T3 and T4 concentrations and the slowed heart rates of the affected mice (Fig. 6A). The hypothyroid mice had markedly reduced serum cGMP concentrations (Fig. 6B), consistent with decreased NOS activity in hypothyroid animals (6,26). Similar amounts of *NOS3* mRNA were present in the bones of hypothyroid and control mice (fig. S6A). Cinaciguat substantially increased the serum cGMP concentrations of treated mice, indicating effective sGC stimulation, but it had no effect on the serum concentrations of T3 or T4 or on heart rate (Fig. 6, A and B).

At seven and four days before euthanasia, mice were injected with calcein to identify newly formed bone on endosteal and trabecular surfaces (Fig. 6, C and D). Control animals had double labeling over 9% of their femoral endosteal surface, whereas hypothyroid mice had only single labeling, indicating a low rate of mineral apposition during the three days between calcein injections (Fig. 6, D and E). Moreover, hypothyroid mice had statistically significantly decreased mineral apposition and bone formation rates (Fig. 6, F and G, and fig. S6, B and C). Cinaciguat restored double calcein labeling and largely restored mineral apposition and bone formation rates in hypothyroid mice, indicating that increased cGMP production could at least partly substitute for TH in supporting osteoblast functions (Fig. 6, D to G, and fig S6, B and C). The hypothyroid mice had decreased serum concentrations of the osteoblast marker pro-collagen1 N-terminal peptide (P1NP) and the osteoclast marker C-terminal telopeptide (CTX) (Fig. 6, H and I). Cinaciguat partly restored P1NP, but did not affect CTX (Fig. 6, H and I). The number of trabecular osteoblasts and osteoclasts was decreased in the hypothyroid mice compared to those in control animals, and cinaciguat partly restored osteoblast numbers, but did not statistically significantly affect osteoclasts (Fig. 6, J and K and fig. S6, D and E). Endocortical osteoid surface and width were reduced in the hypothyroid mice, with a trend toward increased values in cinaciguat-treated animals that did not reach statistical significance (fig. S6, F and G).

Consistent with the NO- and cGMP-dependent anti-apoptotic effects of T3 in osteoblasts and osteocytes in vitro (Fig. 5, E to H, and fig. S5C), osteocytes in the cortical and trabecular bones of hypothyroid mice showed increased apoptosis, with cinaciguat returning the number of apoptotic cells to normal (Fig. 6, L and M and fig. S6, H and I). The amounts of p30-TRα1 protein were similar in membrane extracts from bones of hypothyroid and control mice (fig. S6J). The abundances of mRNAs of the osteoblast differentiation marker osteocalcin (*Bglap2*) and of osteoblast- and osteocyte-derived RANKL (*Tnfsf11*) were reduced in the tibiae of hypothyroid mice compared to those in the tibiae of normal mice, with cinaciguat fully restoring gene expression (Fig. 6N). The abundance of the RANKL antagonist osteoprotegerin (*Tnfrsf11b*) was unchanged under all conditions (Fig. 6N). The T3-dependent production of RANKL in isolated mPOBs was independent of NO (Fig. 5I), but the effect of cinaciguat on RANKL mRNA abundance in hypothyroid mice may be a result of its effects on osteoblast and osteocyte survival. We conclude that decreased bone formation—with reduced osteoblast numbers and activity—and increased osteocyte apoptosis in hypothyroid mice is a result, at least in part, of a relatively NO- and cGMP-deficient state, which may be caused by decreased nongenomic TH signaling.

DISCUSSION

A plasma membrane–associated TRα isoform mediates nongenomic TH signaling

TH rapidly stimulates the generation of second messengers, such as Ca^{2+}, NO, inositol triphosphate, and cAMP in various cells. A membrane-associated member of the TH receptor family has been proposed, but evidence for such a receptor has been lacking (1,2). Instead, the integrin $\alpha_v\beta_3$ was suggested to serve this function (10). Here, we showed that T3 and T4 rapidly activated ERK and Akt at concentrations compatible with binding to a high-affinity TR, and that ERK and Akt activation required TRα, but not TRβ. We discovered a previously uncharacterized 30-kD TRα1 receptor that was necessary and sufficient to mediate T3-induced ERK and Akt activation in multiple cell types. This receptor is palmitoylated and co-localized with caveolin-1 in cholesterol-enriched microdomains in the plasma membrane. Thus, it is positioned to signal through NOS3, PKGII, and Src, which reside in the same membrane microdomains (20,22).

We showed that p30 TRα1 was translated from Met^{150} of TRα1, whereas the mitochondrial 43-kD TRα1 isoform is translated from Met^{39} (17). Alternative translation start sites within a single transcript are conserved in eukaryotic genomes and contribute to proteome diversity, but translation initiation from AUGs more than 50 codons downstream of the first start codon is uncommon (18). The use of alternative translation start sites is thought to occur by leaky ribosomal mRNA scanning, and is typically associated with an unfavorable Kozak consensus sequence around the upstream initiation codon(s), as is the case with TRα. In vitro translation of chicken TRα mRNA in reticulocyte lysates generates peptides of 48, 40, 30, and 27 kD, suggesting that ribosomal scanning and re-initiation occur in vitro as well as in vivo (27). $Met^{120/122}$ and Met^{150} of human TRα are evolutionarily conserved to amphibians, but are absent in TRβ, perhaps explaining why TRβ could not substitute for TRα. The 30- and 33-kD TRα1 isoforms were observed when FLAG-tagged TRα was expressed at concentrations similar to endogenous TRα, suggesting that translation initiation

from $Met^{120/122}$ and Met^{150} was not an artifact of the overexpression of TRα. The peptide initiated from $Met^{120/122}$ was of low abundance in MC3T3 cells, and only p30 TRα initiated from Met^{150} was detected in membranes. Thus, how translational initiation from downstream AUG codons is regulated requires further study. The specificity of the anti-TRα1 antibody that we used was documented in experiments involving siRNA-based depletion and reconstitution of TRα1, but available TRα1-specific antibodies are weak and p30 is not abundant, which may explain why the membrane-associated TRα has not been observed previously. The physiological relevance of the p30 TRα1 isoform is implied by reconstitution experiments in TRα-depleted osteoblasts, because reconstitution with p30 TRα1 partly restored T3-dependent proliferation and fully restored T3-induced NO production, ERK and Akt activation, and cell survival.

Molecular mechanisms of nongenomic TH signaling involving the integrin β3 subunit

We found that T3 rapidly increased the intracellular Ca^{2+} concentration in osteoblasts, leading to increased NO production through NOS3 activation. In addition, we found that T3 activated NOS3 by Akt-mediated phosphorylation of Ser^{1177}, similar to events in endothelial cells (6). The siRNA-mediated depletion of the integrin β_3 subunit blocked T3-induced Akt activation completely, whereas it inhibited NO production by ~50%. We propose that T3 rapidly activates NOS3 by intracellular Ca^{2+} influx and that the resultant stimulation of the NO-cGMP-PKG pathway activates Akt to maintain increased NOS3 activity (Fig. 7).

The T3-dependent activation of ERK and Akt occurred through the NO- and cGMP-dependent activation of PKGII, and required SHP-2, Src, and the integrin β_3 subunit. We showed previously that PKGII phosphorylates and activates the tyrosine phosphatase complex consisting of SHP-1 and SHP-2, which dephosphorylates and activates Src bound to the cytoplasmic tail of β_3 integrin subunits (14). In cooperation with focal adhesion kinase, Src then activates ERK and Akt (15). Activation of Src, ERK, and Akt by TH likely occurs through a similar pathway (Fig. 7), which explains why antibodies that block β_3 integrin subunits and siRNA-mediated depletion of β_3 block TH-induced ERK and Akt activation (1,7,10). Thus, nongenomic TH signaling through p30 TRα converges on a common final pathway that mediates anabolic effects in bone in response to multiple upstream signals, including mechanical stimuli, growth factors, and hormones.

Other workers have observed that T3-induced activation of Akt occurs through the direct interaction of p85 PI3K with either full-length TRα1 or TRβ, depending on the cell type (6,28–31). A mutant $TR\beta^{pv/pv}$ receptor promotes the constitutive activation of PI3K and Akt in thyroid cancer cells, and TRβ colocalizes with p85 in cytosolic and nuclear compartments. Heterologous expression of TRβ in Chinese hamster ovary (CHO) cells reconstituted the PI3K-dependent regulation of a potassium channel at the plasma membrane (30,32). We do not exclude the possibility of parallel pathways that mediate T3-induced Akt activation; however, in osteoblasts, TRβ could not substitute for TRα, and full-length TRα with mutations in $Met^{120/122}$ and Met^{150} did not support nongenomic T3 signaling.

Comparison between thyroid and steroid hormone nongenomic signaling

TRα and TRβ belong to the steroid receptor superfamily, and, similar to sex hormone receptors, are phylogenetically young, being found only in vertebrates. Estrogens, androgens, and progestins exert rapid, nongenomic effects through membrane-bound receptors, with membrane-bound isoforms of estrogen receptor α (ERα) generated by differential mRNA splicing (33). The plasma membrane association of ERα requires its palmitoylation at a cysteine located within a nine amino acid motif that is conserved in most steroid receptors, except for TRα (34). We found that p30 TRα1 is palmitoylated, but that the cysteine(s) necessary for membrane association and nongenomic TH signaling are located N-terminal to the ligand-binding cavity (35). Palmitoylation, protein-protein interaction sites, or both may be obscured by inter-domain interactions in full-length TRα. This would explain why expression of the full-length Mut x3 TRα1 protein did not reconstitute nongenomic TH signaling in TRα-deficient cells.

We found that p30 TRα1 was necessary, but not sufficient, for T3-induced osteoblast proliferation. The full-length Mut x3 TRα1 protein supported some proliferative effects in TRα-depleted osteoblasts, suggesting cooperation between membrane-initiated and nuclear T3 signaling. Similarly, nongenomic estrogen signaling through membrane-associated ER is necessary, but not sufficient, for the pro-proliferative effects of the hormone (34). In contrast, p30 TRα1 fully reconstituted the anti-apoptotic effects of T3 in TRα-depleted osteoblasts, and nongenomic estrogen signaling fully protects osteoblasts from apoptosis in the absence of nuclear signaling (36). Membrane-bound p30 TRα1 appeared as a doublet band on most Western blots, suggesting that it may undergo posttranslational modifications in addition to palmitoylation. ERα undergoes methylation and phosphorylation, which regulate its association with other proteins, and, in endothelial cells, membrane-bound ERα is part of a large, multiprotein “signalosome” that consists of G proteins, NOS3, Src, PI3K, Akt, and scaffolding proteins (33). Thus, nongenomic signaling by ERα, TRα, and possibly other steroid receptor family members is evolutionarily conserved and uses similar mechanisms, converging on Src, ERK, and Akt to affect vital cellular functions.

Importance of nongenomic TH signaling in vivo

Serum TH concentrations are tightly controlled and stable, but tissue T3 concentrations may vary through regulated expression of iodothyronine deiodinases, TH transporters, and TH binding proteins (2). T3 reduces systemic vascular resistance and enhances cardiac contractility within 3 min, providing evidence for nongenomic TH signaling in vivo (37). Regulation of vascular resistance is mediated, at least in part, by the TH-dependent stimulation of endothelial NOS3 (6), and NOS activity in various tissues correlates with the serum concentration of thyroid hormone in rats (26). Our finding of reduced serum cGMP concentrations in hypothyroid mice is consistent with the regulation of NOS activity by TH, although the source of cGMP in serum may include receptor GCs as well as sGCs. We found that the NO-independent sGC stimulator cinaciguat largely reversed the cGMP-deficiency of hypothyroid mice, restoring osteoblastic bone formation and preventing osteocyte apoptosis. These results are in agreement with the NO- and cGMP-dependent effects of TH on osteoblasts and osteocytes observed in vitro, and suggest that nongenomic TH signaling controls bone formation and maintenance. Osteocyte survival is also regulated by

nongenomic estrogen and androgen signaling, and enhanced osteocyte apoptosis contributes to poor bone quality in sex hormone–deficient animals (36).

Clinical relevance of TH signaling in bone

TH binding–deficient TRα1 mutations in humans cause growth retardation and skeletal dysplasia despite the presence of near-normal TH serum concentrations, supporting a role of TRα1 in skeletal development (2). Both hypo- and hyperthyroidism are associated with excess fracture risk, which persists long after reestablishing normal TH serum concentrations (12). Post-menopausal women are especially vulnerable to the skeletal effects of TH excess or deficiency because of the compounding effects of estrogen deficiency on bone. Cinaciguat mimicked the positive effects of TH on bone formation and osteocyte survival without having substantial effects on osteoclasts. These results suggest that agents that enhance cGMP abundance could serve as bone-anabolic agents in states of relative deficiency of NO or cGMP, such as hypothyroidism. By identifying a plasma membrane–localized TR coupled to the NO-cGMP-PKGII pathway, we have contributed to the understanding of nongenomic TH signaling. Because TH is crucial for skeletal development and maintenance, and because animal and clinical studies support the osteogenic functions of NO (38), our results suggest a rationale for using cGMP-enhancing agents to treat osteoporosis.

Materials and Methods

Reagents—Thyroid hormones, calcein, 2-bromo-palmitate, methyl-β-cyclodextrin, 2-hydroxymyristic acid, bromo-deoxyuridine (BrdU), DNAse, and the BrdU-specific antibody were from Sigma. The PI3K inhibitor LY294002 was obtained from Calbiochem. The cGMP agonist 8-(4-chlorophenylthio)-cGMP (8-pCPT-cGMP) and the cGMP antagonist 8-(4-chlorophenylthio)-b-phenyl-1,N2-ethenoguanosine-3’,5’-cyclic monophosphorothioate, Rp isomer (Rp-CPT-PET-cGMPS) were from Biolog. The NOS inhibitor N-nitro-L-arginine methyl ester (L-NAME), and the sGC inhibitor 1*H*-[1,2,4] oxadiazolo[4,3-*a*] quinoxalin-1-one (ODQ) were obtained from Cayman. The sGC activator cinaciguat (BAY 58–2667) was from AdipoGen. Lipofectamine 2000, SYBR-Green PCR Master Mix, and the Ca^{2+}-sensitive fluorescent dye Fura-2 were from Life Technologies. CLS-2 bacterial collagenase type II was obtained from Worthington Biomedical Corporation. [1-^{14}C]-palmitic acid (50 mCi/mmol) was from Moravek Radiochemicals. Antibodies used in this study are listed in table S1.

Plasmid and adenoviral constructs—Full-length rat complementary DNA (cDNA) sequences encoding TRα1 or TRβ1 (a gift of H. Towle, Michigan State University) were cloned in-frame with three C-terminal FLAG epitope tags into pcDNA3 (Life Technologies) (39). N-terminal deletions of 351 or 375 nucleotides (from the first ATG) were generated by PCR, providing the natural Kozak sequences surrounding M120 and M122, or M150, respectively (Fig. 2A). The plasmid encoding NOS3-RFP was purchased from Addgene (# 22497). Site-directed mutagenesis was performed with the QuickChange kit (Stratagene) according to the manufacturer’s instructions. All PCR products were sequenced to ensured the absence of unwanted mutations. Adenoviral vectors encoding β-galactosidase (LacZ), FLAG-tagged or untagged versions of TRα or TRβ (9), and the untagged wild-type or G2A

mutant PKGII (14) were generated with the pAd/CMV/V5-DEST Gateway system (Life Technologies). Typically, cells were infected 24 hours after transfection with siRNA in medium containing 0.1% FBS at an MOI of ~10. After 18 hours, fresh medium with 0.1% FBS was added.

Cell culture and treatments with hormones or drugs—Human POBs (hPOBs) were explant cultures established from trabecular bone fragments obtained from knee replacement operations according to an institutionally approved protocol (13,14). Murine POBs (mPOBs) were isolated from the calvariae of five-to seven-day-old *THRA*$^{f/f}$ and *THRB*$^{f/f}$ mice and from the femurs and tibiae of 8-to 12-week-old *NOS3*$^{f/f}$ mice described below (14). POBs were cultured in Dulbecco's modified Eagle's medium (DMEM) supplemented with 10% fetal bovine serum (FBS). Cells were characterized as described in figs. S1A and S4A and were used at passages 1 to 5. MC3T3-E1 osteoblast-like cells (clone 4) were obtained from the American Type Culture Collection, and were used at <12 passages and cultured in ascorbate-free, α-minimal essential medium (α-MEM) supplemented with 10% FBS (13). Osteocyte-like MLO-Y4 cells were from L. F. Bonewald (University of Missouri-Kansas City), and were grown on collagen-coated plates in α-MEM supplemented with 2.5% enriched calf serum and 2.5% heat-inactivated FBS. Before drug treatment, the medium of sub-confluent cell cultures was changed to phenol red–free medium containing 0.1 or 10% charcoal-stripped FBS (which is referred to as hormone-free medium) for 18 to 24 hours. Cells were pre-incubated with pharmacological inhibitors or vehicle for 30 min, as indicated in the legends. T3 and T4 were made as 10 mM stock solutions in 0.1 N NaOH, diluted into culture medium, and added without exposing cells to fluid shear stress. Control cultures received the same volume of medium.

Mouse experiments—In *THRA*$^{f/f}$ and *THRB*$^{f/f}$ mice, exons 2 and 7 were flanked by loxP sites, respectively, and excision leads to a frame shift. In *NOS3*$^{f/f}$ mice, exons 2 to 9 (*NOS3*) were flanked by loxP sites. POBs were isolated as described earlier, infected with adenovirus encoding CRE recombinase, and the efficiency of CRE-mediated excision of the floxed alleles was determined by reverse transcription polymerase charin reaction (RT-PCR) assay (fig. S1D) or Western blotting analysis (Fig. 4H). Twelve-week-old male C57BL6/J mice were from Jackson Laboratories and received normal mouse chow for 5 days. Half of the mice were then switched to the same chow formulation that was deficient in iodine and contained 0.05% PTU (Harlan Laboratory). After 4 days, mice were randomized to receive daily intra-peritoneal injections of vehicle or cinaciguat (10 μg/kg/day) for 4 weeks. After 2 weeks, heart rates were measured with a tail cuff. At 7 and 4 days before euthanasia, all mice received calcein (25 mg/kg intraperitoneally). Mice were euthanized by CO_2 asphyxiation and exsanguination, and femurs and tibiae were removed and processed as described below. All experiments were approved by the Institutional Animal Care and Use Committee of the University of California, San Diego.

Transfection of cells with DNA and siRNA—Cells were transfected when they had achieved 60 to 80% confluency (for DNA) or 30 to 40% confluency (for siRNA) using 5 μl of Lipofectamine 2000 and a total of 2 μg of DNA or 100 pmol of siRNA in 1 ml of normal serum–containing medium per 6-well dish. Cells were then transferred to hormone-deficient

medium after 6 hours. Experimental treatments occurred 48 hours post-transfection, unless stated otherwise. The sequences targeted by these siRNAs are described in table S2. mRNA knockdown was quantified by real-time RT-PCR in parallel experiments. Protein depletion by the siRNAs targeting PKGI, PKGII, Src, or the β3 integrin subunit was previously shown in MC3T3 cells (14).

Cell fractionation, purification of p30 TRα1-FLAG, T3-agarose pull-downs, and Western blotting analysis—Cells were extracted by Dounce homogenization in lysis buffer [0.25 M sucrose, 20 mM Tricine (pH 7.2), 1 mM EDTA with protease inhibitor cocktail (Calbiochem)], and nuclei and cell debris were removed by centrifugation at 1,000*g* for 10 min. The supernatant was layered over a cushion of 30% Percoll (Sigma Cat# D1644) in lysis buffer, and centrifuged at 84,000*g* for 30 min. The plasma membrane layer was aspirated ("percoll membranes"), and in some experiments, membranes were further fractionated over a discontinuous gradient of 45%−35%−5% Optiprep (Sigma Cat # P1556) after mixing the percoll membranes with 45% Optiprep and centrifuging the gradient at 52,000*g* for 2 hours (40). Twelve 1-ml fractions were collected from the top down, and proteins in each fraction were concentrated by chloroform-methanol precipitation. To purify FLAG-p30 TRα1, human embryonic kidney (HEK) 293T cells transfected with plasmid encoding FLAG-tagged TRα1-Δ149 were lysed in 1% Triton-X-100, 0.1% sodium deoxycholate, 50 mM Tris-HCl (pH 7.5), and protease inhibitor cocktail. After centrifugation at 16,000*g* for 30 min, cleared lysates were incubated with anti-FLAG antibody covalently bound to agarose beads for 15 min on ice. Beads were washed in lysis buffer with 250 mM NaCl, and bound proteins were eluted with FLAG peptide. Purity and protein concentrations were estimated by SDS-PAGE and Coomassie staining, with bovine serum albumin serving as a standard. T3-sepharose and control resin were prepared in parallel with activated CH Sepharose 4B (Sigma-Aldrich) according to a published procedure (41). Briefly, T3 or vehicle (0.1 N NaOH) was added to the washed resin and mixed for 2 hours at room temperature. The suspension was washed three times for 5 min with a solution of 0.1 M Tris-HCl (pH 8.0) and 0.5 M NaCl, and three times with 0.1 M sodium acetate and 0.5 M NaCl (pH 4). Cell membranes were solubilized with 1% Triton-X-100 and 1% NP-40, and incubated for 30 min at 4°C with T3-sepharose or control resin equilibrated with binding buffer containing 1% Triton-X-100, 1% NP-40, 0.25M sucrose, 20 mM Tris-HCl (pH 7.8), 1 mM EDTA, and protease inhibitor cocktail. After six washes, bound proteins were eluted in SDS-sample buffer and analyzed by SDS-PAGE and Western blotting. Western blots were incubated with horseradish peroxidase (HRP)-conjugated secondary antibodies, and protein bands were detected with an enhanced chemiluminescence system, as described previously (13). Films in the linear range of exposure were scanned with Image J software (Wayne Rasband, NIH).

Quantitative RT-PCR assays—RNA was isolated from cells or bone with Trizol reagent (14). Femurs, dissected free of soft tissue, with epiphyses cut off and bone marrow flushed out, were flash-frozen, stored, and pulverized at −80°C. One μg of total RNA was reverse-transcribed, and quantitative PCR was performed with an MX3005P real-time PCR detection system with Brilliant II SYBR Green QPCR Master Mix (Agilent Technologies) (13). Primer sequences are described in table S3. All primers produced a single product and

linear amplification plots. Relative changes in mRNA abundance were determined with the $2^{-\Delta\Delta Ct}$ method, with *glyceraldehyde 3-phosphate dehydrogenase* (*gapdh*) mRNA serving as an internal reference (13). Absolute amounts of TRα and TRβ mRNA were calculated from standard curves from PCR-amplified TRα and TRβ cDNA fragments, respectively, at dilutions corresponding to 10^3 to 10^6 copies.

Preparation of bone cell membrane extracts—Protein extracts were prepared from the bones of control and hypothyroid mice as described previously (42). Frozen bones were pulverized with a mortar and pestle in liquid nitrogen. The bone powder was incubated for 15 min on ice in the following lysis buffer: 50 mM Tris-HCl (pH 8.0), 150 mM NaCl, 2 mM EDTA, 1% Triton X-100, 0.1% SDS, 0.5% sodium deoxycholate, 2 mM $NaVO_4$, 10 mM NaF, plus protease inhibitor cocktail. The samples were centrifuged at 13000*g* for 15 min at 4°C, and 2 ml of supernatant (combined from two femurs and two tibiae per mouse) were concentrated by chloroform-methanol precipitation. The protein pellet was suspended in 100 μl of SDS sample buffer. Proteins were resolved on a 12.5% gel and were analyzed by Western blotting with an anti-TRα1 antibody.

Quantitation of NO_x—NO production was measured based on nitrite and nitrate accumulation in the medium with a two-step colorimetric assay, as previously described (13).

Measurement of intracellular Ca^{2+} concentrations—POBs were plated on glass coverslips and starved for 18 hours in phenol red–free α-MEM containing 0.1% charcoal-stripped FBS. Cells were labeled with 5 μM Fura-2/AM for 30 min at 37 °C. In some experiments, cells were pretreated with 2 mM EGTA for 1 hour and Fura-2 was added during the last 30 min. Cells were gently washed, and fresh hormone-free medium was added before the experiment. The coverslip was carefully lifted out of the culture dish with ~100 μl of medium on top and placed into the inverted microscope chamber (Motic AE31). Cell ensembles were illuminated at wavelengths of 340 and 380 nm, and the emitted light was passed through a 510-nm interference filter and detected by a photomultiplier tube. Images were recorded with the Ionoptix fluorescence system interface and analyzed with Ionwizard 6.3 image analysis software. After recording baseline fluorescence for 3 min, TH, vehicle, or ATP were added in medium containing 2× concentrations taking great care to avoid fluid shear stress. Intracellular Ca^{2+} values were calculated from the 340:380 nm ratio. Fura-2 calibration parameters were determined as previously described (43).

^{14}C-Palmitate incorporation experiments—MC3T3 cells were transfected with empty plasmid or with plasmid encoding FLAG-tagged TRα1-Δ149 and were incubated for 4 hours at 37°C in medium containing 0.1% dialyzed FBS and 50 μCi/ml ^{14}C-palmitic acid (50 mCi/mmol). Cell lysates were subjected to immunoprecipitation with anti-FLAG antibody, and immunoprecipitates were analyzed by SDS-PAGE. Gels were soaked in Fluoro-Hance (Research Products International) and exposed for autoradiography. 1% of the eluates from immunoprecipitates were analyzed separately by Western blotting an with anti-FLAG antibody.

Proximity ligation assay and immunofluorescence staining—MC3T3 cells were plated on glass cover slips in 24-well plates and transfected with 150 ng of plasmid encoding FLAG-tagged TRα1-Δ149 or with 100 ng of plasmid encoding Myc-tagged TRα1-Δ149 together with plasmid encoding NOS3-RFP (NOS-3 C-terminally fused to RFP). After 24 hours, cells were fixed with 3.7% paraformaldehyde, permeabilized in 0.5% Triton-X-100, and blocked in phosphate-buffered saline (PBS), containing 3% bovine serum albumin (BSA). For the proximity ligation assay (PLA), cells transfected with plasmid encoding TRα1-Δ149-FLAG were incubated with murine anti-FLAG antibody (at a 1:1000 dilution) and rabbit anti–caveolin-1 antibody (1:100) together with fluorescein isothiocyanate (FITC)-conjugated phalloidin (1:1000, Life Technologies). PLAs were performed with the Duolink in situ kit (Olink Bioscience) according to the manufacturer's instructions. For immunofluorescence, cells were incubated with rabbit anti-FLAG, murine anti–caveolin-1, or murine anti-Myc antibodies, followed by FITC- or TRITC-labeled secondary antibodies, or both (Jackson Immunoresearch). Nuclei were counter-stained with Hoechst 33342. Cells were viewed with a confocal microscope (Olympus FV1000), a 60/1.42 objective and a 6× digital zoom. Images were analyzed with Fluoview (Olympus) and Photoshop (Adobe) for sizing and contrast adjustment.

BrdU uptake assays—hPOBs were plated on glass coverslips, infected with LacZ or CRE-expressing virus for 24 hours and transferred to hormone-deficient medium for 24 hours before the addition of 1 nM T3 for 30 min. 200 μM BrdU in fresh hormone-deficient medium was then added for 18 hours. Similar results were obtained when T3 was present during the 18-hour BrdU-labeling period. Cells were fixed, permeabilized, and incubated with DNAse I before incubation with an anti-BrdU antibody and Hoechst 33342, as previously described (14).

Measurement of cell death—POBs were infected with CRE- or LacZ-expressing viruses. Twenty-four hours later, cells were transferred to hormone-free medium containing 10% FBS for 24 hours, and some TRα-deficient cells received adenovirus expressing TRα1 to reconstitute the protein. Cells were then incubated for 18 hours with fresh hormone-free medium containing 0.1% (starved) or 10% (control) charcoal-stripped FBS, and were treated with T3 or vehicle as indicated in the figures. A minimum of 200 cells for each condition were examined for trypan blue uptake, and serum starvation–induced cell death was calculated by subtracting the percentage of trypan blue–positive cells in medium containing 10% FBS from the percentage of trypan blue–positive cells in medium containing 0.1% FBS. To detect apoptosis, caspase-3 cleavage was assessed by Western blotting. MLO-Y4 cells received the indicated pharmacological inhibitor or vehicle for 1 hour before being incubated with 1 nM T3 or vehicle for 1 hour. Cells were then treated for 8 hours with 50 μM etoposide, which induces apoptosis by forming a ternary complex with topoisomerase II and DNA, preventing DNA religation, and causing double-stranded DNA breaks. Etoposide-induced cell death was calculated by subtracting the percentage of trypan blue–positive cells in the untreated cultures from the percentage of trypan blue–positive cells in the etoposide-treated cultures.

Osteocyte apoptosis in vivo was quantified by TUNEL staining with the ApopTag Peroxidase In Situ Apoptosis Detection Kit (Millipore, Cat # S7100) on non-decalcified sections. Sections were deplasticized by incubation in 2-methoxyethyl acetate (three times each for 20 min), acetone (twice each for 5 min), and deionized water (twice each for 5 min). Sections were then incubated in 10 mM citrate buffer (pH 7.6) at 98°C for 5 min, which was followed by incubation with 0.5% pepsin in 0.1 N HCl for 30 min at 37°C. The TUNEL reaction (terminal deoxynucleotidyl transferase-mediated biotin-dUTP nick end-labeling) was performed according to the manufacturer's instructions, and slides were counterstained with 0.5% methyl green. A minimum of 200 osteocytes surrounded by bone matrix were counted in either cortical or trabecular bone, and the percentage of TUNEL-positive apoptotic cells with black nuclei was calculated. Microscopic results were confirmed by an independent observer, who counted samples in a blinded fashion.

Bone histomorphometry—Right femurs were fixed in 70% ethanol, dehydrated in graded concentrations of ethanol and xylene, and embedded in methyl methacrylate (without decalcification) at the University of Alabama, Birmingham, Center for Metabolic Bone Disease. Unstained 8-μm thick frontal sections were used for assessing dynamic bone turnover parameters from fluorochrome labeling, and Trichrome-stained sections were used for static parameters. One mouse per experimental group had to be excluded from analysis because of insufficient calcein absorption and inadequate labeling. Slides were scanned with a Hamamatsu Nanozoomer 2.0HT Slide Scanning System, and image analysis was performed with Nanozoomer Digital Pathology NDP.view2 software. All histomorphometric measurements were performed in trabecular bone between 1250 and 250 μm proximal to the growth plate and excluding the cortex, and in cortical bone between 5 and 0.25 mm proximal to the growth plate in distal femurs (as shown in Fig. 6C). Total bone surface (BS), the percentage of single- and double-labeled bone surfaces (sLS and dLS), and interlabel width (average of six measurements per bone) were measured at the endocortical surfaces, as well as on trabecular surfaces in the secondary spongiosa. Mineralizing surface [MS/BS=(dLS + ½ sLS)/BS], mineral apposition rate [MAR=interlabel width/labeling time interval], and bone formation rate [BFR=MAR(MS/BS)] at endosteal and trabecular surfaces were calculated according to convention. A minimal MAR value of 0.3 μm/day was used in PTU-treated animals lacking double labeling (44). Osteoblast and osteoclast numbers were expressed as two-dimensional parameters per mm of bone perimeter (B.Pm), as recommended by the ASBMR Histomorphometry Nomenclature Committee (44). Histomorphometry results were confirmed by an independent, blinded observer.

Measurement of P1NP, CTX, cGMP, T3, and T4 concentrations in mouse serum —Enzyme immune-assays (EIAs) for the quantitative determination of P1NP (Cat # AC-33F1) and CTX (Cat # AC-06F1) in mouse serum were from Immunodiagnostic Systems Inc., and were performed according to the manufacturer's instructions. Similarly, cGMP was measured with an EIA kit from Biomedical Technologies Inc. (Cat # BT-740). Total serum concentrations of T3 and T4 were measured with a solid-phase ^{125}I radioimmunoassay from Siemens Healthcare USA (Cat # TKT31 and Cat # TKT41, respectively).

Data presentation and statistical analyses—Data in bar graphs are the means ± standard error of the mean (SEM) of at least three independent experiments, and Western blots and autoradiographs represent three independent experiments, unless stated otherwise. Graph Pad Prism 5 was used for two-tailed Student t-test (to compare two groups) or one-way ANOVA with Bonferroni post-test analysis (to compare more than two groups). $P < 0.05$ was considered to be statistically significant.

Supplementary Material

Refer to Web version on PubMed Central for supplementary material.

Acknowledgments:

We thank A. Chan and J. Santini for technical assistance, P. Lott for preparing plastic-embedded bone sections, L.F. Bonewald for providing MLO-Y4 cells, and E. Devaney for help with calcium measurements.

Funding: This work was supported by NIH Grants R01AR051300 (to R.B.P.), R01HL066917 (to W.D.), R01AR046797 (to J.A.F.), P30AR04603 (University of Alabama, Birmingham, Center for Metabolic Bone Disease), and P30NS047101 (UCSD Neuroscience Microscopy Shared Facility), VASDHS grant 1I01BX00112 (to W.D.), the P. Robert Majumder Charitable Foundation (to W.D.), and the Deutsche Forschungsgemeinschaft (to R.S.).

REFERENCES AND NOTES

1. Cheng SY, Leonard JL, Davis PJ, Molecular aspects of thyroid hormone actions. Endocr. Rev 31, 139–170 (2010). [PubMed: 20051527]
2. Brent GA, Mechanisms of thyroid hormone action. J. Clin. Invest 122, 3035–3043 (2012). [PubMed: 22945636]
3. Flamant F, Samarut J, Thyroid hormone receptors: lessons from knockout and knock-in mutant mice. Trends Endocrinol. Metab 14, 85–90 (2003). [PubMed: 12591179]
4. Segal J, Ingbar SH, Evidence that an increase in cytoplasmic calcium is the initiating event in certain plasma membrane-mediated responses to 3,5,3’-triiodothyronine in rat thymocytes. Endocrinology 124, 1949–1955 (1989). [PubMed: 2538316]
5. Del VA, Secondo A, Esposito A, Goglia F, Moreno M, Canzoniero LM, Intracellular and plasma membrane-initiated pathways involved in the [Ca2+]i elevations induced by iodothyronines (T3 and T2) in pituitary GH3 cells. Am. J. Physiol Endocrinol. Metab 302, E1419–E1430 (2012). [PubMed: 22414808]
6. Hiroi Y, Kim HH, Ying H, Furuya F, Huang Z, Simoncini T, Noma K, Ueki K, Nguyen NH, Scanlan TS, Moskowitz MA, Cheng SY, Liao JK, Rapid nongenomic actions of thyroid hormone. Proc. Natl. Acad. Sci. U. S. A 103, 14104–14109 (2006). [PubMed: 16966610]
7. Lin HY, Sun M, Tang HY, Lin C, Luidens MK, Mousa SA, Incerpi S, Drusano GL, Davis FB, Davis PJ, L-Thyroxine vs. 3,5,3’-triiodo-L-thyronine and cell proliferation: activation of mitogen-activated protein kinase and phosphatidylinositol 3-kinase. Am. J. Physiol Cell Physiol 296, C980–C991 (2009). [PubMed: 19158403]
8. Mousa SA, O’Connor L, Davis FB, Davis PJ, Proangiogenesis action of the thyroid hormone analog 3,5-diiodothyropropionic acid (DITPA) is initiated at the cell surface and is integrin mediated. Endocrinology 147, 1602–1607 (2006). [PubMed: 16384862]
9. Makino A, Suarez J, Wang H, Belke DD, Scott BT, Dillmann WH, Thyroid hormone receptor-beta is associated with coronary angiogenesis during pathological cardiac hypertrophy. Endocrinology 150, 2008–2015 (2009). [PubMed: 19074585]
10. Bergh JJ, Lin HY, Lansing L, Mohamed SN, Davis FB, Mousa S, Davis PJ, Integrin alphaVbeta3 contains a cell surface receptor site for thyroid hormone that is linked to activation of mitogen-activated protein kinase and induction of angiogenesis. Endocrinology 146, 2864–2871 (2005). [PubMed: 15802494]

11. Hennemann G, Docter R, Friesema EC, de JM, Krenning EP, Visser TJ, Plasma membrane transport of thyroid hormones and its role in thyroid hormone metabolism and bioavailability. Endocr. Rev 22, 451–476 (2001). [PubMed: 11493579]
12. Gogakos AI, Duncan Bassett JH, Williams GR, Thyroid and bone. Arch. Biochem. Biophys 503, 129–136 (2010). [PubMed: 20599658]
13. Rangaswami H, Marathe N, Zhuang S, Chen Y, Yeh JC, Frangos JA, Boss GR, Pilz RB, Type II cGMP-dependent protein kinase mediates osteoblast mechanotransduction. J. Biol. Chem 284, 14796–14808 (2009). [PubMed: 19282289]
14. Rangaswami H, Schwappacher R, Marathe N, Zhuang S, Casteel DE, Haas B, Chen Y, Pfeifer A, Kato H, Shattil S, Boss GR, Pilz RB, Cyclic GMP and protein kinase G control a Src-containing mechanosome in osteoblasts. Sci. Signal 3, ra91 (2010). [PubMed: 21177494]
15. Rangaswami H, Schwappacher R, Tran T, Chan GC, Zhuang S, Boss GR, Pilz RB, Protein Kinase G and Focal Adhesion Kinase Converge on Src/Akt/beta-Catenin Signaling Module in Osteoblast Mechanotransduction. J. Biol. Chem 287, 21509–21519 (2012). [PubMed: 22563076]
16. Koury EJ, Pawlyk AC, Berrodin TJ, Smolenski CL, Nagpal S, Deecher DC, Characterization of ligands for thyroid receptor subtypes and their interactions with co-regulators. Steroids 74, 270–276 (2009). [PubMed: 19073200]
17. Casas F, Rochard P, Rodier A, Cassar-Malek I, Marchal-Victorion S, Wiesner RJ, Cabello G, Wrutniak C, A variant form of the nuclear triiodothyronine receptor c-ErbAalpha1 plays a direct role in regulation of mitochondrial RNA synthesis. Mol. Cell Biol 19, 7913–7924 (1999). [PubMed: 10567517]
18. Bazykin GA, Kochetov AV, Alternative translation start sites are conserved in eukaryotic genomes. Nucleic Acids Res 39, 567–577 (2011). [PubMed: 20864444]
19. Zavacki AM, Harney JW, Brent GA, Larsen PR, Dominant negative inhibition by mutant thyroid hormone receptors is thyroid hormone response element and receptor isoform specific. Mol. Endocrinol 7, 1319–1330 (1993). [PubMed: 8264663]
20. Galbiati F, Razani B, Lisanti MP, Emerging themes in lipid rafts and caveolae. Cell 106, 403–411 (2001). [PubMed: 11525727]
21. Tuomi S, Mai A, Nevo J, Laine JO, Vilkki V, Ohman TJ, Gahmberg CG, Parker PJ, Ivaska J, PKCε regulation of an α5 integrin-ZO-1 complex controls lamellae formation in migrating cancer cells. Sci. Signal 2, ra32 (2009). [PubMed: 19567915]
22. Solomon KR, Danciu TE, Adolphson LD, Hecht LE, Hauschka PV, Caveolin-enriched membrane signaling complexes in human and murine osteoblasts. J. Bone Miner. Res 15, 2380–2390 (2000). [PubMed: 11127203]
23. Schleicher M, Yu J, Murata T, Derakhshan B, Atochin D, Qian L, Kashiwagi S, Di LA, Harrison KD, Huang PL, Sessa WC, The Akt1-eNOS axis illustrates the specificity of kinase-substrate relationships in vivo. Sci. Signal 2, ra41 (2009). [PubMed: 19654415]
24. Kindblom JM, Gevers EF, Skrtic SM, Lindberg MK, Gothe S, Tornell J, Vennstrom B, Ohlsson C, Increased adipogenesis in bone marrow but decreased bone mineral density in mice devoid of thyroid hormone receptors. Bone 36, 607–616 (2005). [PubMed: 15780976]
25. Salloum FN, Das A, Samidurai A, Hoke NN, Chau VQ, Ockaili RA, Stasch JP, Kukreja RC, Cinaciguat, a novel activator of soluble guanylate cyclase, protects against ischemia/reperfusion injury: role of hydrogen sulfide. Am. J. Physiol Heart Circ. Physiol 302, H1347–H1354 (2012). [PubMed: 22268103]
26. Quesada A, Sainz J, Wangensteen R, Rodriguez-Gomez I, Vargas F, Osuna A, Nitric oxide synthase activity in hyperthyroid and hypothyroid rats. Eur. J. Endocrinol 147, 117–122 (2002). [PubMed: 12088928]
27. Bigler J, Hokanson W, Eisenman RN, Thyroid hormone receptor transcriptional activity is potentially autoregulated by truncated forms of the receptor. Mol. Cell Biol 12, 2406–2417 (1992). [PubMed: 1314955]
28. Kenessey A, Ojamaa K, Thyroid hormone stimulates protein synthesis in the cardiomyocyte by activating the Akt-mTOR and p70S6K pathways. J. Biol. Chem 281, 20666–20672 (2006). [PubMed: 16717100]

29. Cao X, Kambe F, Moeller LC, Refetoff S, Seo H, Thyroid hormone induces rapid activation of Akt/protein kinase B-mammalian target of rapamycin-p70S6K cascade through phosphatidylinositol 3-kinase in human fibroblasts. Mol. Endocrinol 19, 102–112 (2005). [PubMed: 15388791]
30. Storey NM, Gentile S, Ullah H, Russo A, Muessel M, Erxleben C, Armstrong DL, Rapid signaling at the plasma membrane by a nuclear receptor for thyroid hormone. Proc. Natl. Acad. Sci. U. S. A 103, 5197–5201 (2006). [PubMed: 16549781]
31. Verga FC, Patriarca V, Bucci B, Mangialardo C, Michienzi S, Moriggi G, Stigliano A, Brunetti E, Toscano V, Misiti S, The TRbeta1 is essential in mediating T3 action on Akt pathway in human pancreatic insulinoma cells. J. Cell Biochem 106, 835–848 (2009). [PubMed: 19160403]
32. Furuya F, Hanover JA, Cheng SY, Activation of phosphatidylinositol 3-kinase signaling by a mutant thyroid hormone β receptor. Proc. Natl. Acad. Sci. U. S. A 103, 1780–1785 (2006). [PubMed: 16446424]
33. Levin ER, Plasma membrane estrogen receptors. Trends Endocrinol. Metab 20, 477–482 (2009). [PubMed: 19783454]
34. Pedram A, Razandi M, Sainson RC, Kim JK, Hughes CC, Levin ER, A conserved mechanism for steroid receptor translocation to the plasma membrane. J. Biol. Chem 282, 22278–22288 (2007). [PubMed: 17535799]
35. Wagner RL, Apriletti JW, McGrath ME, West BL, Baxter JD, Fletterick RJ, A structural role for hormone in the thyroid hormone receptor. Nature 378, 690–697 (1995). [PubMed: 7501015]
36. Kousteni S, Bellido T, Plotkin LI, O'Brien CA, Bodenner DL, Han L, Han K, DiGregorio GB, Katzenellenbogen JA, Katzenellenbogen BS, Roberson PK, Weinstein RS, Jilka RL, Manolagas SC, Nongenotropic, sex-nonspecific signaling through the estrogen or androgen receptors: dissociation from transcriptional activity. Cell 104, 719–730 (2001). [PubMed: 11257226]
37. Schmidt BM, Martin N, Georgens AC, Tillmann HC, Feuring M, Christ M, Wehling M, Nongenomic cardiovascular effects of triiodothyronine in euthyroid male volunteers. J. Clin. Endocrinol. Metab 87, 1681–1686 (2002). [PubMed: 11932301]
38. Jamal SA, Hamilton CJ, Nitric oxide donors for the treatment of osteoporosis. Curr. Osteoporos. Rep 10, 86–92 (2012). [PubMed: 22210559]
39. Belke DD, Gloss B, Swanson EA, Dillmann WH, Adeno-associated virus-mediated expression of thyroid hormone receptor isoforms-alpha1 and -beta1 improves contractile function in pressure overload-induced cardiac hypertrophy. Endocrinology 148, 2870–2877 (2007). [PubMed: 17317766]
40. Smart EJ, Ying YS, Mineo C, Anderson RG, A detergent-free method for purifying caveolae membrane from tissue culture cells. Proc. Natl. Acad. Sci. U. S. A 92, 10104–10108 (1995). [PubMed: 7479734]
41. Scapin S, Leoni S, Spagnuolo S, Fiore AM, Incerpi S, Short-term effects of thyroid hormones on Na+-K+-ATPase activity of chick embryo hepatocytes during development: focus on signal transduction. Am. J. Physiol Cell Physiol 296, C4–12 (2009). [PubMed: 18829895]
42. Watkins M, Grimston SK, Norris JY, Guillotin B, Shaw A, Beniash E, Civitelli R, Osteoblast connexin43 modulates skeletal architecture by regulating both arms of bone remodeling. Mol. Biol. Cell 22, 1240–1251 (2011). [PubMed: 21346198]
43. Grynkiewicz G, Poenie M, Tsien RY, A new generation of Ca2+ indicators with greatly improved fluorescence properties. J. Biol. Chem 260, 3440–3450 (1985). [PubMed: 3838314]
44. Dempster DW, Compston JE, Drezner MK, Glorieux FH, Kanis JA, Malluche H, Meunier PJ, Ott SM, Recker RR, Parfitt AM, Standardized nomenclature, symbols, and units for bone histomorphometry: a 2012 update of the report of the ASBMR Histomorphometry Nomenclature Committee. J. Bone Miner. Res 28, 2–17 (2013). [PubMed: 23197339]

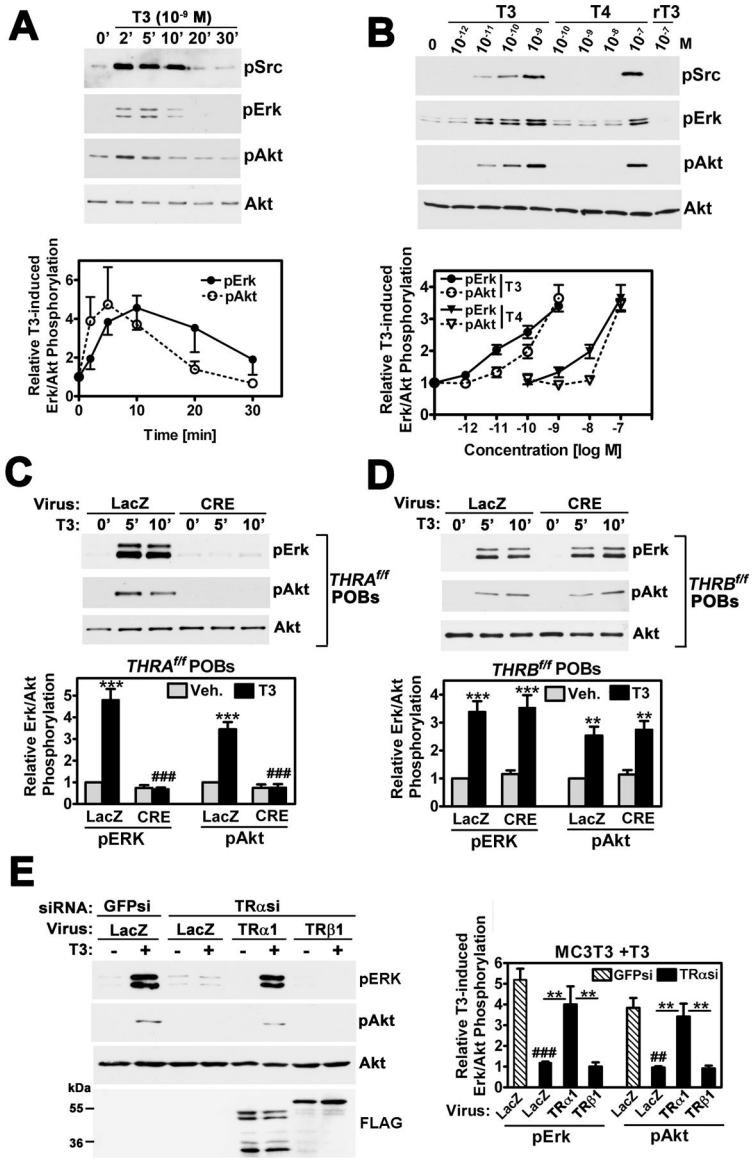

Fig. 1. Nongenomic TH signaling requires a TRα isoform.

(**A** and **B**) Human POBs in hormone-deficient medium containing 0.1% FBS were incubated with (A) 1 nM T3 for the indicated times or (B) the indicated concentrations of T3, T4, or reverse T3 (rT3) for 10 min. Src, ERK, and Akt phosphorylation was assessed by Western blotting analysis with antibodies specific for Src ($pTyr^{418}$), ERK½ ($pTyr^{204}$), and Akt ($pSer^{473}$). Equivalent loading was determined by analyzing blots for total Akt protein. Line graphs below the blots show means ± SEM of the fold-changes in pERK and pAkt abundances. Data are from three to five independent experiments. (**C** and **D**) POBs isolated from *THRA*$^{f/f}$ or *THRB*$^{f/f}$ mice were infected with control (LacZ-expressing) or CRE-expressing viruses. Forty-eight hours later, the cells were treated with vehicle or 1 nM T3 for 5 or 10 min. Phosphorylation of ERK and Akt was assessed as described for (A) and (B). The bar graphs show data for the 10-min time points, with vehicle-treated, control virus–infected cells assigned a value of 1. Data are means ± SEM from three independent

experiments. $^{**}P < 0.01$, $^{***}P < 0.001$ compared to vehicle-treated cells; $^{\#\#\#}P < 0.001$ compared to T3-treated, control virus–infected cells. (**E**) MC3T3 cells were transfected with siRNAs specific for GFP or TRα and then were infected with viruses encoding LacZ, FLAG-tagged TRα1, or FLAG-tagged TRβ1. Cells were treated with vehicle or T3 for 10 min. Knockdown efficiency is shown in Fig. 2B and fig. S1G. Virus expression was assessed by Western blotting of cell lysates with an anti-FLAG antibody. Bar graph shows means ± SEM of the relative amounts of pERK and pAkt in the indicated samples. Data are from three independent experiments. $^{\#\#}P < 0.01$, $^{\#\#\#}P < 0.001$ compared to cells transfected with GFP-specific siRNA; $^{**}P < 0.01$ for the indicated comparison.

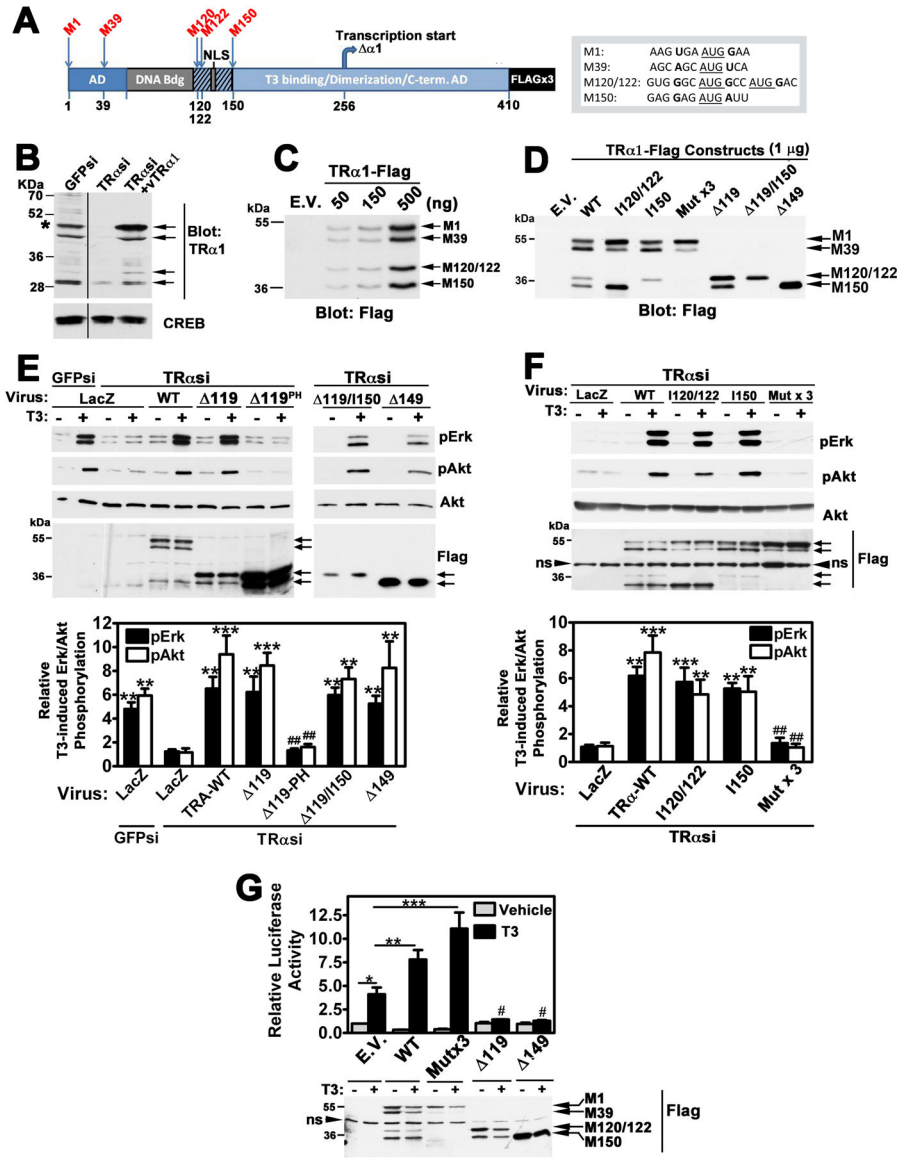

Fig. 2. Identification of previously uncharacterized TRα isoforms and of their function in nongenomic TH signaling.

(**A**) Diagram of the 410-amino-acid TRα1 protein showing the transcription activation domain (AD), DNA-binding (Bdg) domain, nuclear localization signal (NLS), and a C-terminal domain mediating T3=binding, receptor dimerization, and transcriptional activation. Putative translation initiation sites are indicated (M), as is the TH binding-incompetent TRΔα1 isoform transcribed from an intronic promoter. Met^{150} (M150) follows a flexible “hinge” region. Nucleotide sequences surrounding methionine codons are shown on the right and are conserved between mouse and human. (**B**) MC3T3 cells were transfected with siRNAs targeting GFP or TRα, and then were infected with virus encoding either LacZ or native (untagged) TRα1. Fourtyeight hours later, cell lysates were analyzed by Western blotting with antibodies against the C-terminus of TRα1 or CREB (loading control). Non-contiguous lanes from a single blot are shown and are separated by vertical lines. The asterisk indicates full-length TRα1; the blot is respresentative of three

experiments. (**C**) MC3T3 cells were transfected with empty vector (E.V.) or the indicated amounts of plasmid encoding C-terminally FLAG-tagged TRα1 and then were analyzed by Western blotting with an anti-FLAG antibody. (**D**) MX3T3 cells were transfected with plasmids encoding the following constructs: full-length wild type TRα1 (WT); full-length receptor with isoleucine substituted for $Met^{120/122}$ or Met^{150} (I120/122 or I150, respectively); full-length receptor with Met^{120}, Met^{122}, and Met^{150} mutated to isoleucines (Mut x3,); TRα1 from which codons 1 to 119 are deleted (Δ119); the Δ119 construct in which Met^{150} is mutated to isoleucine (Δ119/I150); TRα1 from which codons 1 to 149 were deleted (Δ149). Samples were analyzed by Western blotting with anti-FLAG antibody. Peptides translated from Met^{1}, Met^{39}, $Met^{120/122}$, and Met^{150} are indicated. Note that the triple-FLAG tag causes proteins to migrate with a higher apparent molecular mass (see fig. S2D; data are representative of five experiments). (**E** and **F**) MC3T3 cells were transfected with siRNAs targeting GFP (first two lanes) or TRα (all other lanes), and then were infected with viruses encoding the TRα1 constructs described in (C). $Δ119^{PH}$ refers to a TH-binding–deficient mutant (P398H). Cells were treated with vehicle or 1 nM T3 treatment for 10 min and then were analyzed by Western blotting to determine ERK and Akt activation as described for Fig. 1, A and B. Western blots were analyzed with anti-FLAG antibody to determine the extent of viral infection. ns, nonspecific. Graphs show means ± SEM of the fold-increase in the abundances of pERK and pAkt from three independent experiments. Cells that were transfected with GFP-specific siRNA, infected with control virus, and treated with vehicle were assigned a value of 1. $^{**}P < 0.01$, $^{***}P < 0.001$ compared to cells transfected with TRα-specific siRNA and infected with control virus; $^{\#\#}P < 0.05$ compared to cells transfected with TRα-specific siRNA and infected with virus encoding WT TRα. (**G**) MC3T3 cells were cotransfected with a TRE-containing luciferase reporter plasmid and with empty vehicle or with plasmids encoding the indicated TRα1 constructs described in (C). Cells were then treated with vehicle or T3 for 24 hours. Data in the bar graph are means ± SEM of the relative luciferase activities in the indicated samples and are from five independent experiments. $^{*}P < 0.05$, $^{**}P < 0.01$, $^{***}P < 0.001$ for the indicated comparisons; $^{\#}P < 0.05$ compared to cells transfected with empty plasmid and treated with T3.

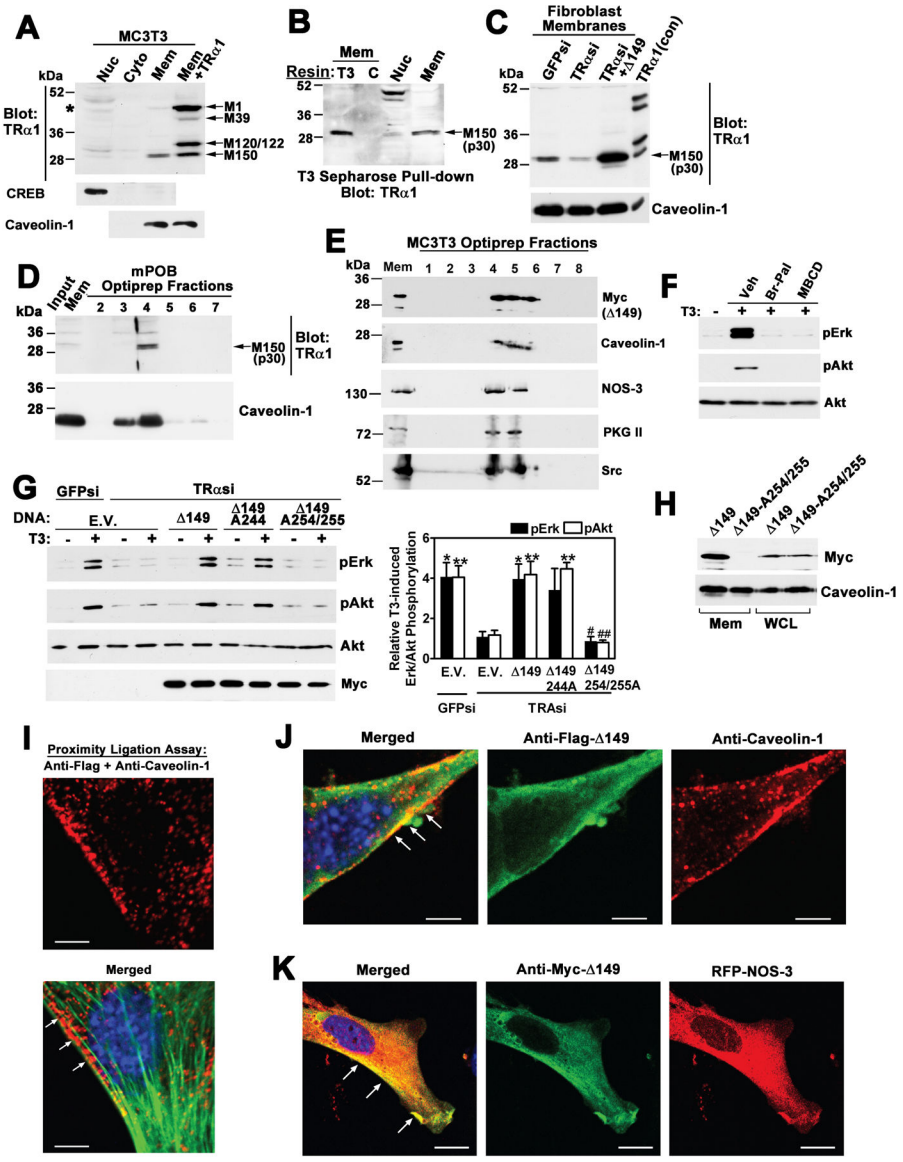

Fig. 3. Membrane association of p30 TRα1 and co-localization with caveolin-1 and NOS3.

(A) Nuclear (Nuc), cytosolic (Cyto), and membrane (Mem) fractions of MC3T3 cells were analyzed by Western blotting with antibodies against the TRα1 C-terminus, CREB, or caveolin-1. Extracts of cells transfected with plasmid encoding non-tagged, WT TRα1 added to membranes (Mem+TRα1) served as a positive control. The asterisk indicates full-length TRα1. Analysis of concentrated nuclear extracts is shown in fig. S2A. (B) Solubilized membranes were incubated with T3-sepharose (T3) or control-sepharose (C), and bound proteins were analyzed by Western blotting with anti-TRα1 antibody. (10% of input is shown, representative of three experiments). (C) NIH-3T3 fibroblasts were transfected with siRNAs specific for GFP or TRα, and some cells were transfected with plasmid encoding nontagged TRα1-Δ149. Samples were analyzed by Western blotting as described for (A). (D) Murine POB membranes were fractionated over an Optiprep density gradient, and fractions of increasing density were analyzed by Western blotting with anti-

TRα1 and anti-caveolin-1 antibodies (representative of two experiments). (E) Membranes from MC3T3 cells transfected with Myc-tagged TRα1-Δ149 were fractionated as described for (D) and were analyzed by Western blotting for the presence of the indicated proteins (representative of three experiments). (F) hPOBs were pre-treated with vehicle, 10 μM 2-bromo-palmitate (Br-Pal), or 10 mM methyl-β-cyclodextrin (MBCD) before being treated with 1 nM T3. The extent of ERK and Akt activation was assessed by Western blotting as described for Fig. 1A (representative of three experiments). (G) MC3T3 cells were transfected with siRNAs specific for GFP or TRα as well as with empty vector (E.V.) or with plasmids encoding the indicated TRα1 constructs. The cells were then treated with vehicle or T3 and analyzed by Western blotting as described for (F). Detection of Myc-tagged constructs is shown in the lower blot. Bar graph shows means ± SEM of the relative amounts of pERK and pAkt from four independent experiments. $^{*}P < 0.05$, $^{**}P < 0.01$ compared to cells transfected with TRα-specific siRNA and E.V; $^{\#}P < 0.05$, $^{\#\#}P < 0.01$ compared to cells transfected with plasmid encoding TRα1-Δ149. (H) Cells were transfected with plasmids encoding Myc-tagged TRα1-Δ149 or TRα1-Δ149-$A^{254/255}$. Plasma membranes (Mem) or whole-cell lysates (WCL) were prepared and analyzed by Western blotting with anti-Myc and anti-caveloin-1 antibodies (representative of three experiments). (I) MC3T3 cells transfected with plasmid encoding FLAG-tagged TRα1-Δ149 were incubated with mouse anti-FLAG and rabbit anti-caveolin-1 antibodies followed by a proximity ligation assay. The close proximity of p30 TRα1 and caveolin produced punctate red fluorescence. Cells were co-stained with FITC-labeled phalloidin and Hoechst 33342 (to stain the nucleus), and were analyzed by fluorescence microscopy. Scale bar: 2.5 μm. (J and K) Cells were transfected with (J) plasmid encoding FLAG-tagged TRα1-Δ149 or (K) plasmids encoding Myc-tagged TRα1-Δ149 and RFP-tagged NOS3. Cells were incubated with antibodies against the indicated proteins, DNA was stained with Hoechst, and the cells were analyzed by fluorescence microscopy. Scale bar: 2.5 μm; data are representative of three experiments.

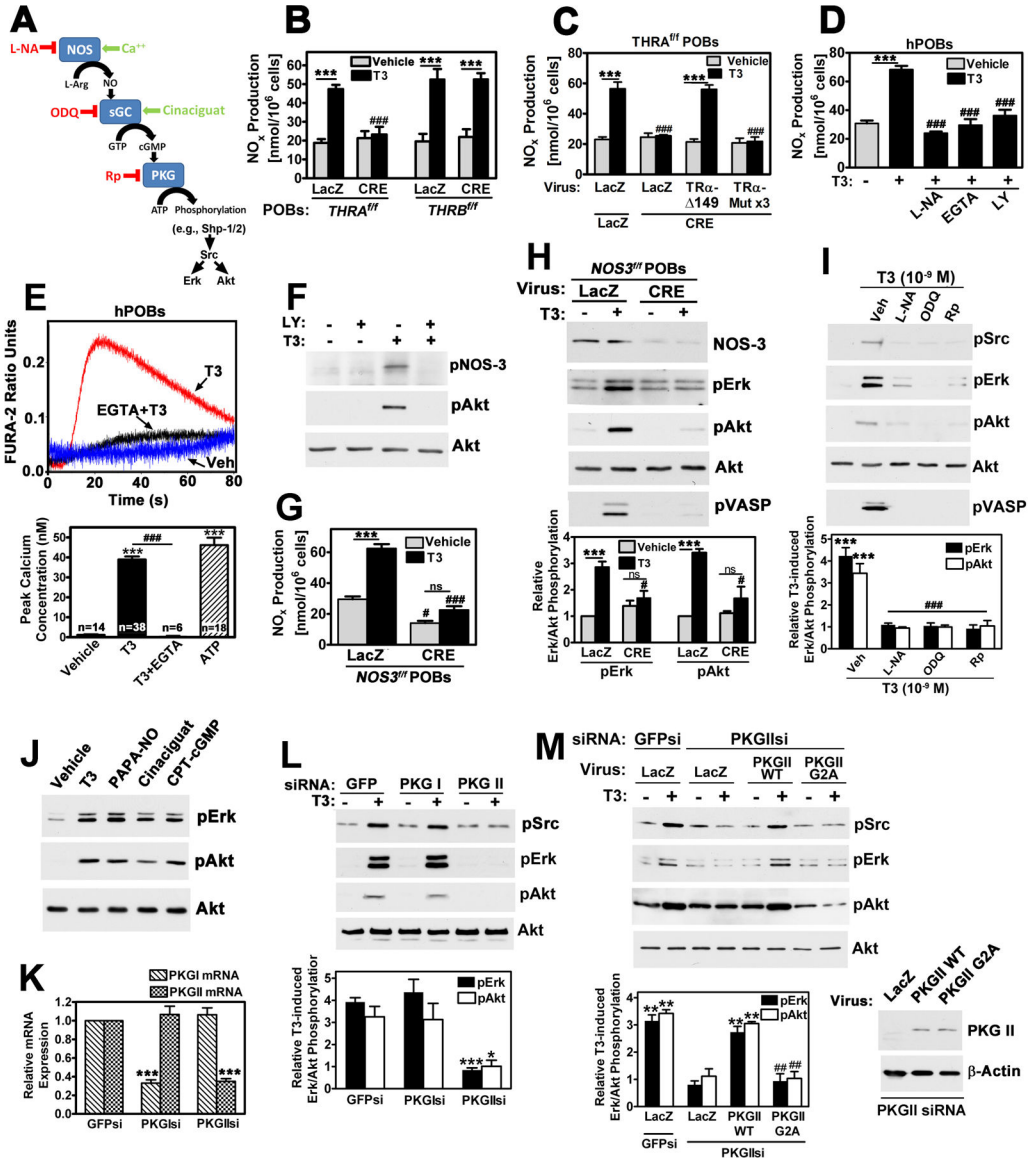

Fig. 4. The activation of Src, ERK, and Akt by TH requires NOS3 and membrane-bound PKGII.

(**A**) Diagram of the NO-cGMP signaling cascade, with enzyme inhibitors in red and activators in green. Src activation by SHP-1 or SHP-2 leads to ERK and Akt activation (14). (**B** to **D**) POBs isolated from (B and C) *THRA*$^{f/f}$ or *THRB*$^{f/f}$ mice were infected with LacZ- or CRE-expressing viruses. (C) In addition, cells were transfected with plasmids encoding the indicated TRα1 constructs. Forty-eight hours later, cells were treated with vehicle or 1 nM T3 for 10 min. (D) Human POBs were incubated for 30 min with 4 mM L-NAME (L-NA), 2 mM EGTA, or 10 μM LY294002 (LY) before being treated with vehicle or T3. Stable NO oxidation products (NOx represents nitrite and nitrate) were measured with the Griess reagent. Data are means ± SEM from three or four independent experiments. ***$P < 0.001$ compared to vehicle-treated cells, $^{\#\#\#}P < 0.001$ compared to cells infected with control virus and treated with T3). (**E**) Fura-2AM–loaded hPOBs that were not pretreated or were pretreated with 2 mM EGTA were incubated with vehicle or 1 nM T3 at time zero.

Intracellular Ca^{2+} mobilization was calculated from the 340:380 nm Fura-2 fluorescence ratio, and representative traces are shown. The bar graph shows means ± SEM of the peak Ca^{2+}concentrations in the indicated numbers of cells. ATP served as a positive control. ***$P < 0.001$ compared to vehicle-treated cells; ###$P < 0.001$ compared to cells treated with T3 alone. (**F** and **H**) *NOS3*$^{f/f}$ POBs were treated as described for (B). (F) Cells were then analyzed to measure NO production. (H) Cell lysates were analyzed by Western blotting as described for Fig. 1A with antibodies against the indicated proteins. Phosphorylated VASP was used as a positive control for PKG activation. Bar graphs show means ± SEM from three or four independent experiments. ***$P < 0.001$ compared to vehicle-treated cells; #$P < 0.05$, ###$P < 0.001$ compared to cells infected with control virus and treated with vehicle. Ns, not significant. (**G**) hPOBs were left untreated or were treated with LY294002 before being treated with vehicle or T3. The presence of phosphorylated NOS3 ($pSer^{1177}$) and Akt ($pSer^{473}$) was determined by Western blotting analysis, representative of three experiments. (**I**) hPOBs were pretreated with 4 mM L-NAME, 10 μM ODQ, or 50 μM Rp-CPT-PET-cGMPS (Rp) before being incubated with vehicle or 1 nM T3. Western blotting analysis was performed to determine the phosphorylation of Src, ERK, Akt, and VASP as described for (H). Bar graph shows means ± SEM from three to five independent experiments. ***$P < 0.001$ compared to vehicle-treated cells; ###$P < 0.001$ compared to cells treated with T3 alone. (**J**) hPOBs were treated with 1 nM T3, 10 μM PAPA-NONOate, 100 nM cinaciguat, or 100 μM 8-pCPT-cGMP for 10 min. Cells were then analyzed by Western blotting with antibodies against the indicated proteins, data are representative of three experiments. (**K** to **M**) MC3T3 cells were transfected with siRNAs specific for GFP, PKGI, or PKGII. (M) Cells were also infected with viruses encoding LacZ, WT PKGII, or mutant PKGII that cannot bind to the plasma membrane (G2A). Cells were treated with vehicle or T3 and were analyzed as described for (H). (K) The relative abundances of PKGI and PKGII mRNAs were quantified by RT-PCR analysis. (L and M) Cell lysates were analyzed by Western blotting with antibodies against the indicated proteins. Bar graphs in (L) and (M) show means ± SEM of the relative abundances of pERK and pAkt from three independent experiments. *$P < 0.05$, ***$P < 0.001$ compared to cells treated with GFP-specific siRNA in (K) and (L); **$P < 0.01$ compared to cells treated with GFP-specific siRNA and infected with control virus and ##$P < 0.01$ compared to cells expressing WT PKGII in (M).

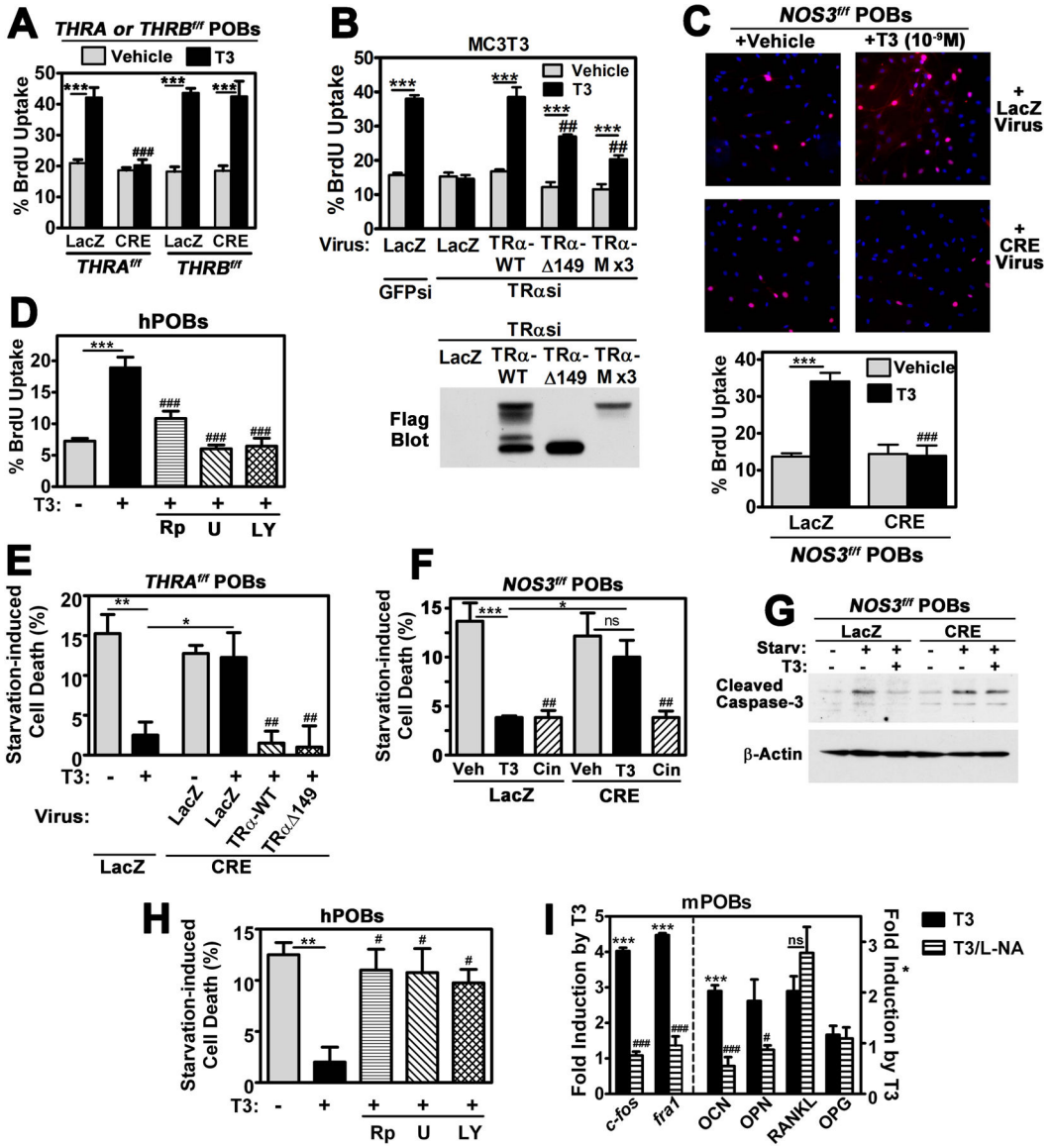

Fig. 5. Nongenomic TH signaling through the p30 TRα1–NO–cGMP pathway regulates cell proliferation and survival.

(**A** and **B**) Effect of nongenomic TH signaling on cell proliferation. (A) POBs isolated from *THRA*$^{f/f}$ and *THRB*$^{f/f}$ mice were infected with LacZ- or CRE-encoding adenoviruses. (B) MC3T3 cells were transfected with siRNAs targeting GFP or TRα and then were infected with adenoviruses encoding LacZ or the indicated TRa1 constructs, as described for Fig. 2. After 24 hours in hormone-free medium with 0.1% FBS, cells were treated with vehicle or 1 nM T3 for 30 min before being incubated with 8-Br-deoxyuridine (BrdU) in hormone-free medium for 18 hours. The percentages of cells that were labeled with BrdU were determined by immunofluorescence staining. (**C**) POBs from *NOS3*$^{f/f}$ mice were infected with LacZ- or CRE-encoding adenoviruses. BrdU in S-phase nuclei was assessed as in B. DNA was counter-stained with Hoechst. (A to C) Data in bar graphs show means ± SEM of the percentages of BrdU-labeled cells from four independent experiments. ***$P < 0.001$ compared to vehicle-treated cells; $^{\#\#}P < 0.1$, $^{\#\#\#}P < 0.001$ compared to cells infected with

control virus and treated with T3. (**D**) hPOBs were treated with 50μM Rp-CPT-PET-cGMPS (Rp), 10 μM U0126 (U), or 10 μM LY294002 (LY) for 1 hour before being incubated with vehicle or T3. BrdU uptake was determined as described for (A). Data are means ± SEM of the percentages of BrdU-labeled cells from four independent experiments. $^{***}P < 0.001$ compared to vehicle-treated cells; $^{\#\#\#}P < 0.001$ compared to cells treated with T3 alone. (**E** to **G**) Effect of nongenomic TH signaling on cell death. (E) POBs from *THRA*$^{f/f}$ mice were infected with LacZ-encoding virus or with viruses expressing the indicated TRα constructs as described for (A). (F and G) *NOS3*$^{f/f}$ mice were infected with LacZ- or CRE-expressing viruses as described for (A). (E to G) Cells were then subjected to serum-deprivation for 18 hours in the presence or absence of (E to G) 1 nM T3 or (F) 1 nM T3 or 100 nM cinaciguat (Cin). Cell death was assessed by (E and F) trypan blue uptake or (G) Western blotting analysis for cleaved caspase-3. Bar graphs show means ± SEM of the percentages of dead cells from three or four independent experiments. $^{*}P < 0.05$, $^{**}P < 0.01$, $^{***}P < 0.001$ compared to cells infected with LacZ-encoding virus and treated with T3; $^{\#\#}P < 0.01$ for cells infected with LacZ-encoding virus compared to cells infected with TRα-encoding virus and treated with T3 (E) and for cinaciguat-treated compared to vehicle-treated cells in (F). (**H**) hPOBs were treated as described for (D), starved of serum, and analyzed as described for (E). Data are means ± SEM of the percentages of dead cells from four independent experiments. $^{**}P < 0.001$ compared to vehicle-treated cells, $^{\#}P < 0.05$ compared to cells treated with T3 alone. (**I**) mPOBs were treated with vehicle or 1 nM T3 in the presence or absence of 4 mM L-NAME (L-NA) for 1 hour (left, undifferentiated cells) or 24 hours (right, differentiated cells). The relative abundances of the mRNAs for *c-Fos*, *Fosl1*, osteocalcin (*Bglap2*), osteopontin (*Spp1*), RANKL (*Tnfsf11*), and osteoprotegerin (*Tnfrsf11b*) were quantified by RT-PCR analysis and were normalized to that of *HGPRT* mRNA. The mean abundance of each transcript measured in vehicle-treated cells was assigned a value of one. Data are means ± SEM of the fold-increase in the indicated mRNA from three to six independent experiments. $^{***}P < 0.001$ for T3-treated cells compared to vehicle-treated cells; $^{\#}P < 0.05$, $^{\#\#\#}P < 0.001$ compared to cells treated with T3 alone.

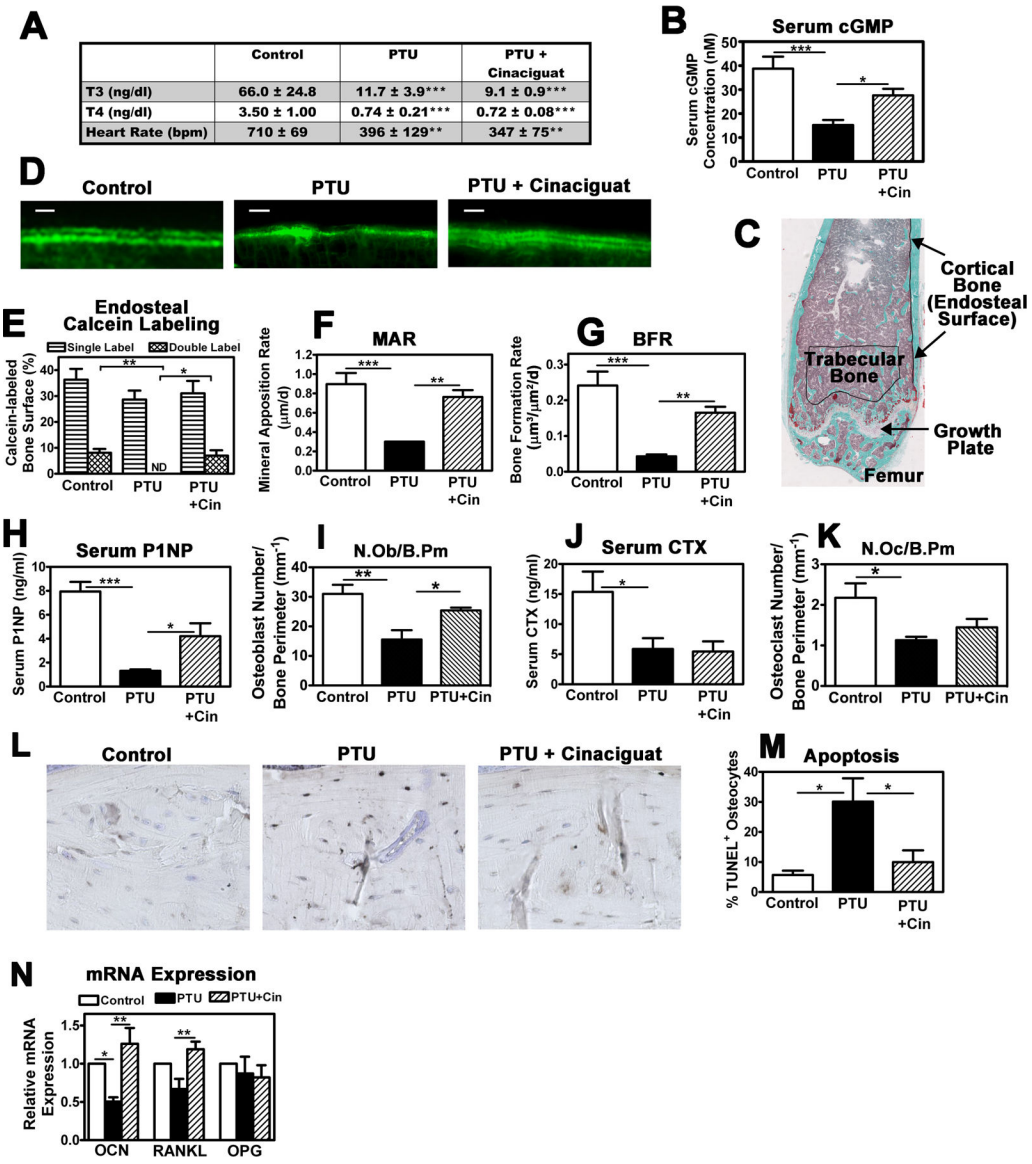

Fig. 6. Hypothyroid mice are cGMP-deficient, but increasing their cGMP concentration improves bone formation and prevents osteocyte apoptosis.

Twelve week-old male C57BL6 mice were fed a control diet or an iodine-deficient diet containing 0.15% PTU for 4 weeks. During this time, mice received daily injections of either vehicle or cinaciguat (10 μg/kg). Calcein was injected 7 and 4 days before euthanasia. (**A**) Heart rate was measured 2 weeks after starting the diet, whereas serum T3 and T4 concentrations were measured at the time of euthanasia. Data are means ± SEM from seven mice for each condition. *$P < 0.05$, **$P < 0.01$, ***$P < 0.001$ compared to mice fed a control diet. (**B**) Serum cGMP concentrations were measured 2 hours after the last injection with cinaciguat. Data are means ± SEM from seven mice for each condition. *$P < 0.05$, ***$P < 0.001$ for the indicated comparisons. (**C**) Endosteal cortical bone surface and the area analyzed for trabecular bone are indicated by a black line on a trichrome-stained distal femur. (**D**) Femoral endosteal calcein labeling was assessed by fluorescence microscopy. Scale bar: 10 μm. (**E**) Single- and double-labeled surfaces were measured on fluorescence

microscopy photographs, and were expressed as a percentage of the total endosteal bone surface assessed between 0.25 and 5 mm from the growth plate. ND, not detected. (**F**) Mineral apposition rate (MAR) and (**G**) bone formation rate (BFR) were calculated from the inter-label distances. Data in (E) to (G) are means ± SEM from six mice for each condition. $*P < 0.05$, $**P < 0.01$, $***P < 0.001$ for the indicated comparisons. A minimal MAR value of 0.3 μm/day was assigned to the PTU group, which showed only single-labeled surfaces. (**H and I**) Serum concentrations of procollagen-1 N-terminal peptide (P1NP) and C-terminal telopeptide (CTX) for the indicated mice were measured by ELISA. (**J and K**) The numbers of osteoblasts (N.Ob, J) and osteoclasts (N.Oc, K) per mm of trabecular bone perimeter (B.Pm) were counted for the indicated mice. Data in (H) to (K) are means ± SEM from six mice for each condition. $*P < 0.05$, $**P < 0.01$, $***P < 0.001$ for the indicated comparisons. (**L**) Apoptotic osteocytes were identified in cortical bone by TUNEL staining (black nuclei). Data are representative of four mice per group. (**M**) Bar graph shows means ± SEM of the percentages of TUNEL+ osteocytes from four mice for each group. (**N**) RNA was extracted from femurs from the indicated mice, and the relative abundances of osteocalcin (*Bglap1*), RANKL (*Tnfsf11*), and osteoprotegerin (*Tnfrsf11b*) mRNAs were quantified by RT-PCR analysis and normalized to that of GAPDH mRNA. Mean values of the control group were assigned a value of one. Data are means ± SEM from five or six mice for each condition. $*P < 0.05$, $**P < 0.01$, for the indicated comparisons.

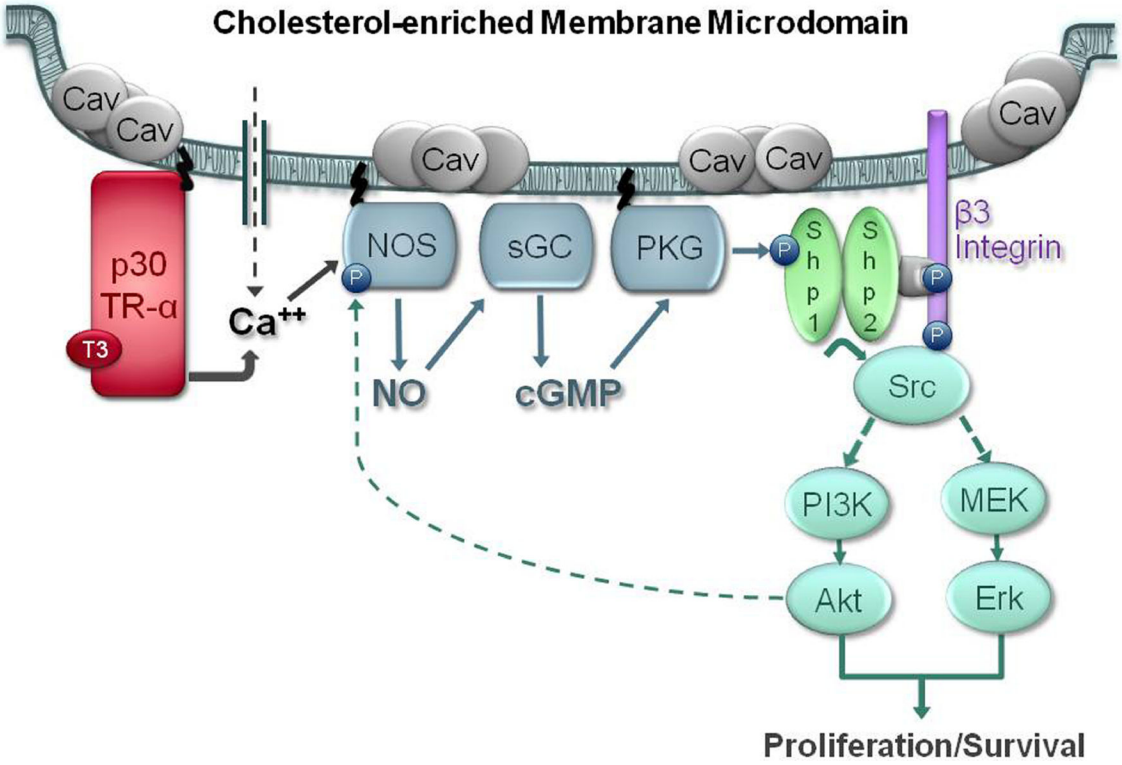

Fig. 7. Proposed mechanism of nongenomic TH signaling by p30 TRα1.

Binding of T3 to the plasma membrane–associated p30 TRα1 induces an increase in intracellular Ca^{2+} concentration, which leads to activation of the NO-cGMP-PKGII signaling cascade and the phosphorylation and activation of the SHP-1–SHP-2 phosphatase complex. This complex is bound, together with Src, to the cytoplasmic tail of the integrin β_3 subunit (14). Src is activated by SHP-1–SHP-2 and initiates activation of MEK-ERK and PI3K-Akt signaling, which results in enhanced cell proliferation and survival. Lipid modifications important for the membrane-association of p30 TRα1, NOS3, and PKGII are in black.